Dielectrophoretic Characterization and Separation of Leukocytes

by

YAĞMUR YILDIZHAN

Submitted to
the Graduate School of Engineering and Natural Sciences
in partial fulfillment of
the requirements for the degree of
Master of Science

SABANCI UNIVERSITY

July 2018

DIELECTROPHORETIC CHARACTERIZATION AND SEPARATION OF LEUKOCYTES

Yağmur Yıldızhan

APPROVED BY

Asst. Prof. Dr. Meltem Elitaş (Thesis Supervisor) .....

Asst. Prof. Dr. Murat Kaya Yapıcı .....

Assoc. Prof. Dr. Ali Özhan Aytekin .....

DATE OF APPROVAL: .....

ABSTRACT

DIELECTROPHORETIC CHARACTERIZATION AND SEPARATION OF LEUKOCYTES

YAĞMUR YILDIZHAN

Mechatronics Engineering M.Sc. Thesis, July 2018

Thesis Supervisor: Asst. Prof. Dr. Meltem Elitaş

Keywords: Dielectrophoresis, Carbon-Electrodes, Monocytes, Macrophages, DEP Separation, Fluorescent Labeling, Membrane Folding Factor

Characterization and separation of leukocytes are critical for precision in medical diagnostics, treatment and biomedical research. Existing characterization and separation methods are generally based on centrifugation or antibody-mediated recognition assays. Even though these methods are highly sensitive and specific, they are sometimes inefficient and require several preparative steps involving heavy equipment. Moreover, antibody labeling might cause biases during characterization and change the cell phenotype, particularly for immunological cells that can quickly respond and adapt to environmental changes. Dielectrophoresis (DEP) has a great potential for noninvasive manipulation of cells based on their dielectric characteristics. It is a favorable alternative to the current cell manipulation methods by being label-free, low-cost, fast and accurate. In this thesis, dielectrophoretic characterization of U937 monocytes, macrophages, dead cells and monocytes stained with commercially available fluorescent dyes are presented using a 3D carbon-electrode DEP device. Also, a new DEP model is proposed, and dielectrophoretic characterization of leukocytes and RBCs were performed using the proposed model. Then, live-dead leukocytes and monocytes-macrophages were separated successfully based on differences between their dielectric properties, while preserving their viability. This approach will reduce the dead cell contamination risk in blood analyses and increase the precision in disease diagnostics by achieving more reliable and accurate test results.

ÖZET

AKYUVARLARIN DİELEKTROFORETİK KARAKTERİZASYONU VE AYRIŞTIRILMASI

YAĞMUR YILDIZHAN

Mekatronik Mühendisliği Yüksek Lisans Tezi, Temmuz 2018

Tez Danışmanı: Dr. Ögr. Üyesi Meltem Elitaş

Anahtar Kelimeler: Dielektroforezis, Karbon-Elektrot, Monosit, Makrofaj, DEP Ayrıştırma, Florosan Etiketlemesi, Hücre Zarı Katlanma Katsayısı

Akyuvarların karakterizasyonu ve ayrıştırılması medikal teşhisin, tedavilerin ve biyomedikal araştırmalarının doğruluğu için kritiktir. Mevcut karakterizasyon ve ayrıştırma yöntemleri genel olarak santrifüje ya da antikora bağımlı teşhise dayandırılmaktadır. Bu yöntemler oldukça hassas ve spesifik olmalarına rağmen bazen yetersiz kalıp ağır ekipmanlar içeren çeşitli hazırlık adımları gerektirir. Üstelik antikor etiketlemesi karakterizasyon sırasında bazı eğilimlere sebep olabilir ve özellikle ortam değişimine hızlıca cevap veren ve adapte olabilen bağışıklık hücrelerinin fenotipini değiştirebilir. Dielektroforezis (DEP) hücrelerin dielektrik özelliklerine dayalı olarak noninvazif manipülasyonları için büyük potansiyel taşımaktadır. Var olan hücre manipülasyon yöntemlerine kıyasla etiket gerektirmediği, düşük maaliyetli, hızlı ve kesin olduğu için tercih edilen bir alternatiftir. Bu tezde U937 monositlerin, makrofajların, ölü hücrelerin ve piyasada satılan florosan boyalarla boyanmış hücrelerin üç boyutlu karbon-elektrot DEP cihazı kullanılarak dielektroforetik karakterizasyonları sunulmuştur. Ayrıca yeni bir DEP modeli öngörülmüş ve bu model kullanılarak akyuvar ile alyuvarların dielektroforetik karakterizasyonu gerçekleştirilmiştir. Sonrasında, canlı-ölü akyuvarlar ve monosit-makrofajlar dielektrik özelliklerindeki farklılıklara göre, canlılıklarını koruyarak başarılı bir şekilde ayrıştırmıştır. Bu yaklaşım kan analizlerinde ölü hücre kontaminasyon riskini azaltacak ve daha güvenilir, kesin test sonuçları sağlayarak hastalık teşhisinde doğruluğu arttıracaktır.

≪ To My Beloved Family ≫

ACKNOWLEDGEMENTS

I would like to express my sincere gratitude to the following people for their invaluable contributions to this study and my life:

Dr. Meltem Elitaş for being my advisor and for giving me the opportunity of stepping into the worlds of cell biology and microfluidics. I would like to thank her not only for providing scientific insight and support, but also challenging me to become the best version of myself.

My jury members: Dr. Ali Özhan Aytekin and Dr. Murat Kaya Yapıcı for their insight, constructive feedback and valuable time.

My collaborators for sharing their equipment, valuable ideas, experience and time: Dr. Rodrigo Martinez-Duarte, Monsur Islam, Didem Özkazanç, Yunus Akkoç and Omid Babaie Rizvandi.

All the members of the Biomechatronics group and my friends: Doğukan Kaygusuz, Ekin Yağış, Zain Fuad, Alara Altay, Umut Barş Göğebakan and Nurdan Erdem for helping me both intellectually and emotionally and especially for making the place fun. And of course Hande Karamahmutoğlu, my partner in crime for these two years, who is extremely fun and has been there for me throughout this journey.

My roommate Esra Becan, for all the precious night long chats, her wisdom and cute little notes.

My best friend Betül Urgancı, for her constant emotional support, sharing my love for literature and intellectual conversations even there are oceans between us.

And last but not least, I would like to thank my family. My mother Navruz Yıldızhan and my father Muharrem Yıldızhan, for all their endless love and support, for always believing in me and continuously providing love for education and taught me the importance of standing on my own feet. They are the greatest gift that I have in my life.

Thank you all.

Table of Contents

List of Figures

List of Tables

Chapter 1

Introduction

1.1 Motivation

Characterization and selective manipulation of blood cell subpopulations are critical for precision in medical diagnostics, treatment and biomedical research [17]. Characterization of these cells can provide valuable information to guide regenerative and personalized medicine, and particularly cancer therapy [18]. Moreover, the purity of cell subpopulations is critical in treatment and diagnosis that demand high-quality, accurate, and repeatable measurement techniques and tools [19]. There are many methods available for cell identification and separation ranging from density-based approaches to antibody-mediated recognition assays. Most density-based methods are based on centrifugation [20], and they are more often preferred at the population level than the single cell analysis. On the other hand, fluorescent-activated (FACS) [21] and magnetic-activated (MACS) [22] cell sorting techniques are the most common cell-sorting methods and rely on well-defined biochemical markers and immunolabeling procedures. FACS uses fluorescent labels that can interact with antigens on the cell surface or within the cell interior to identify target cells and MACS relies on magnetic microbeads coated with antibodies that attach to the cells of interest for separation. Eventhough these methods are highly sensitive and specific, they are sometimes inefficient and require several preparative steps involving heavy equipment such as centrifuges, large magnets, and flow cytometers.

These additional steps are considered to be time-consuming, and the required equipment is expensive. Moreover, cell labeling might cause biases during characterization and change the cell phenotype, particularly for immunological cells that can quickly respond and adapt to environmental changes.

Thus, there is a need for new manipulation devices that will eliminate the drawbacks of the existing ones and can characterize and separate cells while preserving the genotype and phenotype of the cells to resemble the status of the diseases. The emerging label-free cell characterization and separation techniques are mainly based on the dielectric properties of the cell populations. Dielectrophoresis (DEP), the motion of polarizable particles in a non-uniform electric field, has been extensively studied for many years [23–25]. It has a great potential for noninvasive manipulation of cells based on their dielectric characteristics. It is a favorable alternative to the current cell manipulation methods by being label-free, low-cost, fast and accurate.

DEP has been implemented in several cell characterization and separation studies. In one of the early applications, DEP was used to separate topoietic stem cells expressing the CD34 + antigen from peripheral blood and bone marrow [26, 27]. Becker *et al.* showed the separation of human breast cancer cells from general leukocyte populations, preserving cell viability [28]. One of the recent DEP studies demonstrated the characterizaztion of human skeletal stem and bone cell populations [29].

1.2 Contributions of the Thesis

This study aims to separate human leukocytes without altering their genetic or phenotypic properties using a 3D carbon-electrode dielectrophoresis (DEP) device. In the first part of this research, human leukocytes were characterized to investigate the dielectrophoretic responses of the cells under different conditions. Pre- and post-labeled single cells were stained with commercially available fluorescent dyes were characterized to investigate whether these dyes alter the DEP responses of cells. Furthermore, blood cells were numerically characterized to compare existing experimental outcomes with DEP theory. In the second part of the thesis, live and dead leukocytes were separated to reduce dead-cell contamination from the cell populations to achieve accurate and reliable readouts from biological assays and clinical tests. Also, monocytes and monocyte differentiated macrophages were separated using a 3D carbon-electrode DEP device. These are two of the subsets of leukocytes known for their high levels of plasticity and functional diversity. This study strongly suggests the accuracy of dielectrophoresis as a manipulation tool for the separation of cells that are highly heterogeneous and share similar dielectric properties.

1.3 Outline of the Thesis

Chapter 2 explains the dielectrophoresis phenomenon, the dielectrophoretic force, the Clausius-Mossotti factor, dielectric polarization and dielectric properties of cells. It then presents a literature survey on dielectrophoretic studies of cells. **Chapter 3** introduces the 3D carbon-electrode DEP device, explains the cell preparation, immunophenotyping of the cells and how the images were acquired and analyzed. Also, it demonstrates and details the experimental setup and procedure. **Chapter 4** presents the results of dielectrophoretic characterization experiments, the numerical study for the characterization of leukocytes and RBCs and finally discusses the results. **Chapter 5** is about the experimental results of dielectrophoretic separation experiments. Separation of live-dead cells and monocytes-macrophages are presented and discussed. **Chapter 6** concludes the thesis and details possible applications of 3D carbon-electrode DEP device for future work.

1.4 Publications

- Y. Yildizhan, U. B. Gogebakan, A. Altay, M. Islam, R. Martinez-Duarte, M. Elitas. Quantitative investigation for dielectrophoretic effect of fluorescent dyes at single-cell resolution. **ACS Omega**, 2018; 3 (7), 7243-7246.
- Y. Yildizhan, N. Erdem, M. Islam, R. Martinez-Duarte, M. Elitas. Dielectrophoretic Separation of Live and Dead Monocytes Using 3D Carbon-Electrodes. **Sensors**, 2017; 17 (11): 2691.
- N. Erdem, Y. Yildizhan, M. Elitas. (2017). A numerical approach for dielectrophoretic characterization and separation of human hematopoietic cells. **International Journal of Engineering Research and Technology (IJERT)**, 6 (4), 1079-1082.
- Yildizhan, M. Islam, R. Martinez-Duarte, M. Elitas. Dielectrophoretic Separation of Live and Dead Monocytes Using 3D Carbon-Electrodes. Journal Paper **(in preparation)** .

Chapter 2

Theory and Literature Review

Dielectrophoresis (DEP) is undoubtedly one of the fundamental concepts of microfluidic manipulation. There are numerous studies and technologies developed implementing DEP since Herb Pohl first proposed its definition in 1951 [30]. It is primarily a robust method for identification and separation of cell subpopulations in heterogeneous microenvironments without the need for biochemical labeling. Nevertheless, there are still challenges, and limitations need to be overcome and there is a room for potential future applications especially in medical diagnostics.

In this chapter, the dielectrophoresis phenomenon will be explained by detailing the dielectrophoretic force and the Clausius-Mossotti Factor to describe the polarizability of the bioparticles. Then, we will focus on the dielectric properties of cells to investigate the direct relevance to the prediction and interpretation of their dielectrophoretic behavior. Finally, we will outline the dielectrophoretic studies of bioparticles as a literature review to demonstrate the progress of dielectrophoresis in biomedical applications.

2.1 Dielectrophoresis

2.1.1 Dielectrophoretic Force

Dielectrophoresis (DEP) is the motion of polarizable particles in a non-uniform electric field, which generated from direct current (DC) or alternating current (AC) potentials. Figure 2.1 illustrates the electric field distribution around a particle both for uniform and non-uniform electric fields. There are two cases in each condition; one is where the particle is more polarizable than the surrounding medium, and the other is when the particle is less polarizable. Figure 2.1 (a) demonstrates a particle that is more polarizable than its surrounding in a uniform electric field, where the electric field lines bend towards the particle, and the Figure 2.1 (b) demonstrates a particle that is less polarizable than its surrounding in a uniform field, where the electric field lines bend around the particle. If there were no polarisability difference between the particle and the surrounding medium, electric field lines would be continuous and act like there were no particle [31].

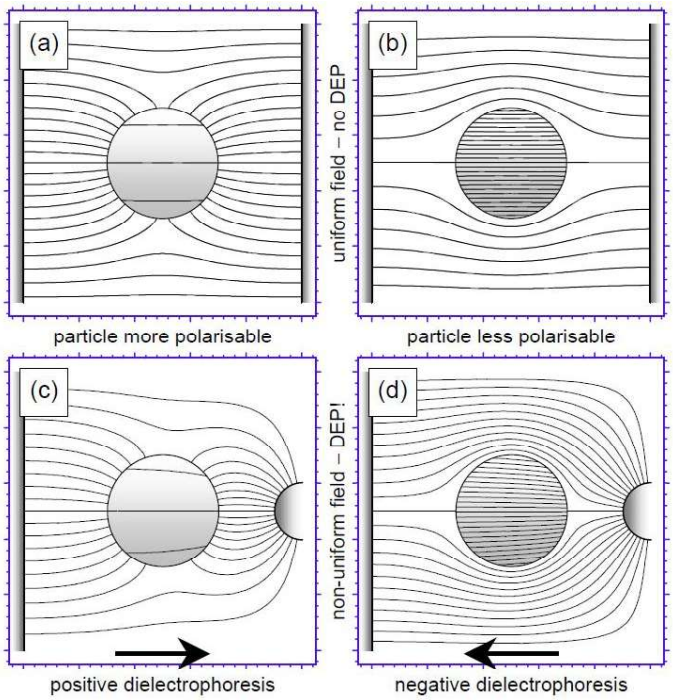

FIGURE 2.1: Numerically calculated electric field lines. Image acquired from [1].

When there is a non-uniform electric field, the particles behave similarly, yet the density of electric field lines changes. The electric field lines in one side become denser than the other side, and the imbalance of forces on the induced dipole moves the particle. If the polarizability of a particle is higher than the suspending medium as in Figure 2.1 (c), the direction of the dipole will be towards to the high electric field region, and the particle will feel an attractive force, called positive dielectrophoresis (pDEP), and will start to move towards the electrode. On the other hand, if the polarizability of a particle is less than the suspending medium as in Figure 2.1 (d), the direction of the dipole will be opposite to the high electric field region, and the particle will feel a repulsive force, called negative dielectrophoresis (nDEP), and will start to move away from the electrode. Conclusively, the force on the induced dipole defined as the dielectrophoretic force and demonstrated as:

$$\langle \vec{F}_{DEP} \rangle = 2\pi R^3 \varepsilon_0 \varepsilon_m Re[K(\omega)] \nabla E^2 \tag{2.1}$$

where R is the radius of the particle, ε_0 is the permittivity of free space (8.854×10^{-12} Fm^{-1}), ε_m is the relative permittivity of the suspending medium, $Re[K(\omega)]$ is the real part of the Clausius-Mossotti Factor, ω is the radian ferquency of the applied electric field and ∇E is the electric field gradient.

The Clausius-Mossotti (CM) relation is named after the Italian physicist Ottaviano Mossotti and the German physicist Rudolf Clausius, and the factor derived from solving Laplaces equations. The CM factor for a homogeneous spherical particle is given as:

$$CM = \frac{\varepsilon_p^* - \varepsilon_m^*}{\varepsilon_p^* + 2\varepsilon_m^*} \tag{2.2}$$

where ε_p^* is the complex permittivity of the particle and ε_m^* is the complex permittivity of the suspending medium. The complex permittivity defined as:

$$\varepsilon^* = \varepsilon + \sigma/(j\omega) \tag{2.3}$$

where ε is the permittivity of the particle or medium, σ is the conductivity of the particle or medium, ω is the radian ferquency of the applied electric field and j is $\sqrt{-1}$.

The applied voltage does not affect the direction of the DEP force (2.1). Although, the frequency of the applied electric field can alter the polarizability of the cells and the medium because of the CM factor (2.2) dependency. Furthermore, the radius of a particle directly affects the DEP force as well as the dielectric properties (permittivity and conductivity) of a particle, which solely arises from the CM factor.

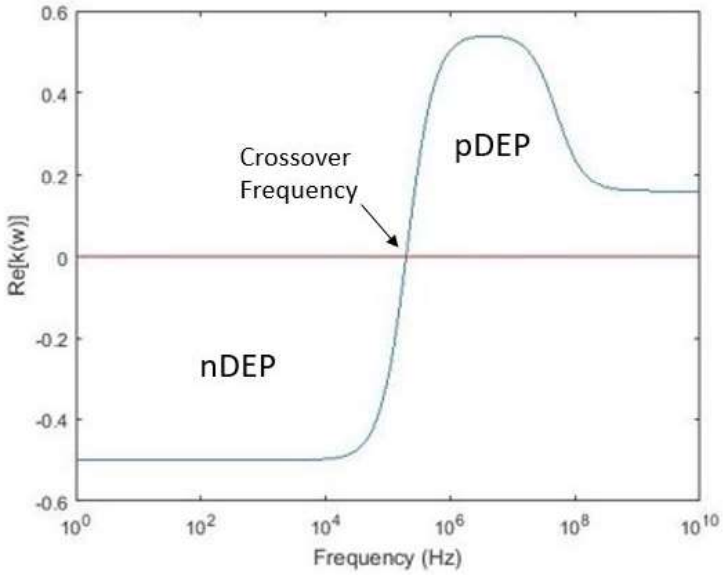

FIGURE 2.2: The real (Re) component of the Clausis-Mossotti factor as a function of frequency (Hz), created using the MATLAB program.

When the real part of the CM factor is equal to zero at a particular frequency, DEP force acting on the particle becomes zero, and the particle does not move. This specific frequency is known as the "crossover frequency". The crossover frequency acts as a signature of the particle and has an essential role in cell separation processes. Figure 2.2 illustrates the real part of the Clausius-Mossotti factor as a function of frequency (Hz) and demonstrates the possible motives of a particle under DEP force; nDEP, pDEP and crossover, which are detailed above.

2.1.2 Dielectric Properties of Cells

The dielectric behavior of cells is theorized based on Maxwell-Wagener and shell models [32]. The Maxwell-Wagner relation elucidates charge build-up that arises in layered dielectric material interfaces depending on the difference of charge carrier relaxation times in these dielectrics. Permittivity and conductivity parameters describe each cell as well as the components (nucleus, organelles, cytoplasm, and membrane) of the cells. All of these parameters requires a complex formulation for the shell model (Figure 2.3). That is why the single shell model eliminates the other parameters except for the cell membrane and cytoplasm and accepts the cell as a complete sphere.

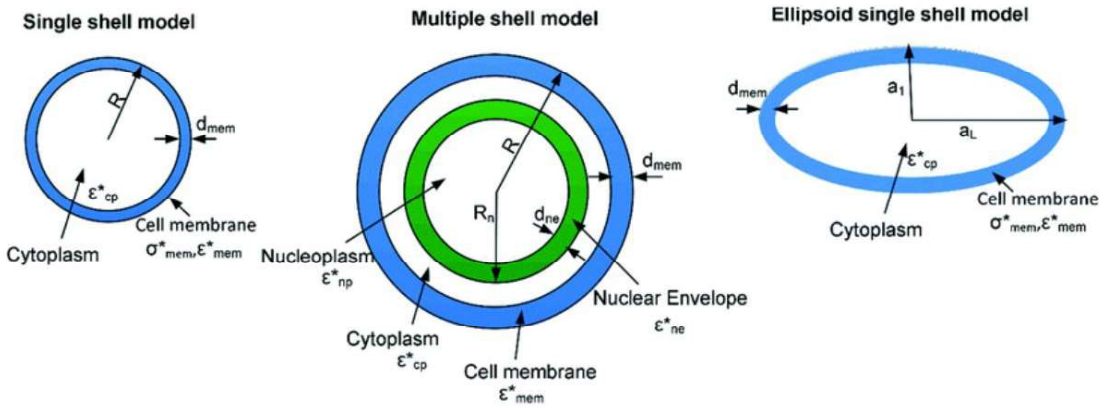

FIGURE 2.3: Cell shell models. Image retrieved from [2].

While deriving CM factor for cell mixtures, effective permittivity (ε_{eff}) is used to define a spherical volume of a cell suspension instead of particle permittivity, because cells are non-homogenous complex structures with a non-uniform distribution of insulating and conducting biochemical components [2]. Then the real part of the Clausius-Mossotti factor is calculated as:

$$CM = \frac{\varepsilon^*_{eff} - \varepsilon^*_m}{\varepsilon^*_{eff} + 2\varepsilon^*_m} \tag{2.4}$$

when based on the single shell model (ε^*_{eff}) is described as:

$$\varepsilon^*_{eff} = \varepsilon^*_{mem} \frac{(\frac{r}{r-d})^3 + 2\frac{\varepsilon^*_{int} - \varepsilon^*_{mem}}{\varepsilon^*_{int} + 2\varepsilon^*_{mem}}}{(\frac{r}{r-d})^3 - \frac{\varepsilon^*_{int} - \varepsilon^*_{mem}}{\varepsilon^*_{int} + 2\varepsilon^*_{mem}}} \tag{2.5}$$

where d is the thickness of the cellular membrane, ε^*_{mem} is the complex permittivity of the membrane and ε^*_{int} is the complex permittivity of the cytoplasm.

2.2 Dielectrophoretic Studies of Cells

Many DEP separation devices have been developed to sort a wide range of cell subpopulations. Main approaches can be categorized as classic metal electrode-based DEP [33], insulator-based DEP (iDEP) [34] and contactless DEP (cDEP) [35].

The classic metal electrode DEP devices have been demonstrated to be effective for characterizing and separating blood cells [36], cancer cells [37] and stem cells [33]. Typically they are formed of an array of platinum or gold electrodes deposited on a glass or a silicon substrate positioned on the planar surface of a flow channel to generate a non-uniform electric field [4]. Electric field density in metal electrodes is commonly higher at edges of the electrodes and it decreases with the distance.

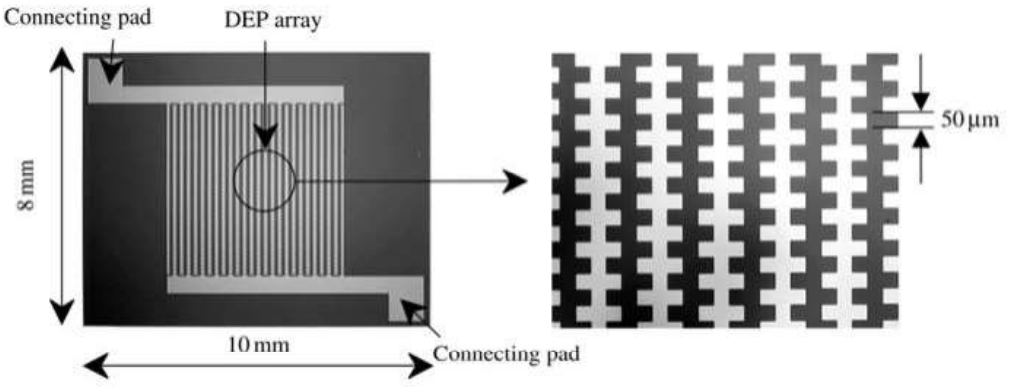

FIGURE 2.4: Photographs of DEP chip demonstrating electrode and spacing dimensions. Image acquired from [3].

One example of classic metal electrode DEP was consisted of a flip-chip DEP layer containing platinum interdigitated electrodes. The electrode and spacing dimension was $50\mu m$ with $8mm \times 10mm$ dize size and $5mm \times 5mm$ electrode area as demonstrated in figure 2.4. The microfluidic channels of the chip was $1.27mm$ wide and the fluidic chamber was $3.5mm$ wide for DEP collection and separation. The dimensions of the final packaged DEP device was $40 \times 40mm^2$ with $4.6mm$ thickness. Figure 2.5 demonstrates the DEP effect and separation of different bacteria populations from blood cells. The red blood cells were trapped under 10 Vpp bias, 10 kHz in the areas between the electrodes while *B. cereus* cells were trapped at the electrode edges and surfaces, and *E. coli* cells and *L. monocytogenes* were trapped in the center of the electrodes. Up to 97 % separation efficiency was achieved and the device was proposed as a potential sample complexity reducer for detection of infectious disease pathogens and biological warfare agents [3].

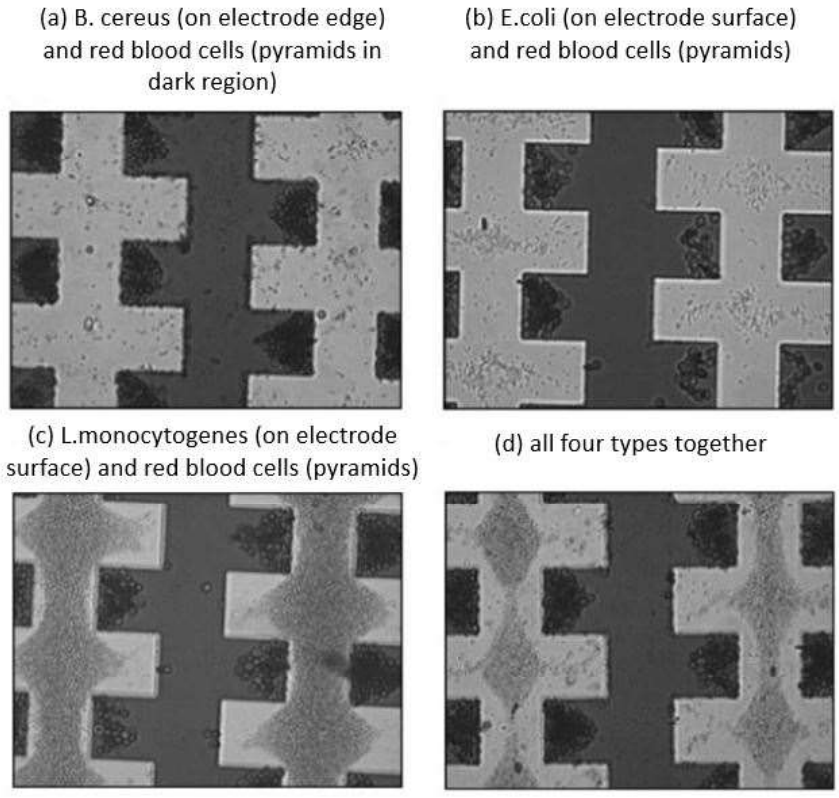

FIGURE 2.5: The separation of bacteria from blood with an electrode-based dielectrophoresis polymer laminate device operating at 10 kHz, 10 Vpp. Image acquired and reproduced from [4],[3].

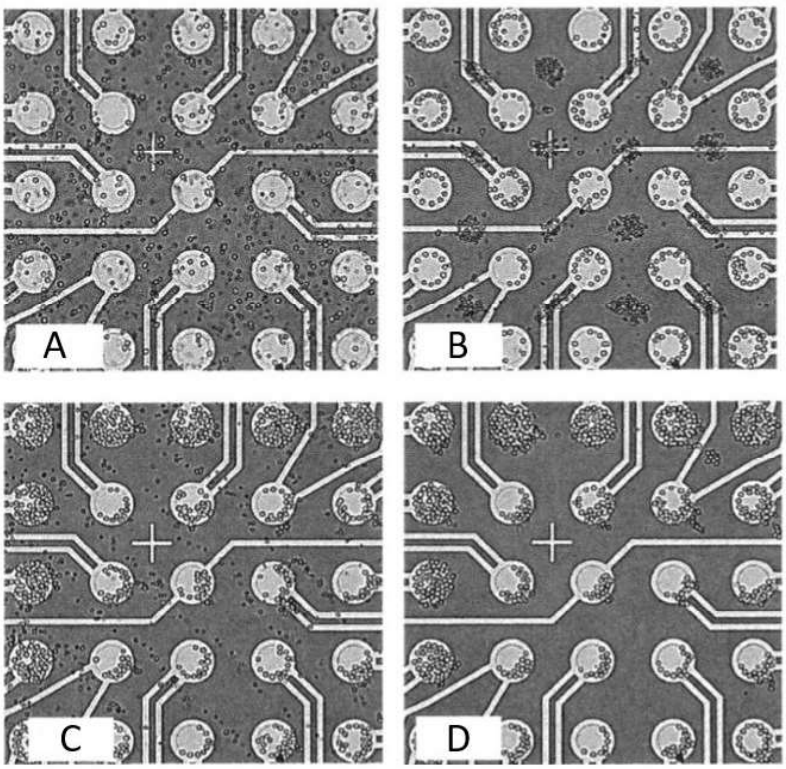

FIGURE 2.6: The DEP separation for U937 and PBMC mixture operating at 500 kHz, 7 Vpp. Image acquired and reproduced from [5]

.

Another study by Huang *et al.* implemented 5×5 array of circular, platinum electrodes for both cell separation and gene expression profiling [5]. The array was fabricated on a silicon wafer using standard semiconductor processing techniques. It was consisted of 25 circular, platinum electrodes with $80\mu m$ diameter and $200\mu m$ center to center spacing. Final device had $450\mu m$ thickness and $\sim 7.5\mu l$ volume. U937 monocytes or human T-cell leukemia virus type 1 (HTLV-1) tax-transformed cells (Ind-2) were separated from PBMC and neuroblastoma cells (SH-SY5Y) were separated glioma cells (HTB) with 95 % separation efficiency, which is independent of the number of input cells. The separation process of U937 monocytes and PBMC mixture is presented above. The mixture was introduced to the array as in figure 2.6.A. After 500 kHz, 7 Vpp was applied for 5 minutes U937 monocytes were collected on the electrodes (pDEP) as in figure 2.6.B. and PBMC were assembled between the electrodes (nDEP). Then, the buffer was introduced with 40 $\mu l/min$ rate while the

electric field was still on. Finally, as seen in figure 2.6.D. PBMC were washed away with the given flow and U937 cells were retained on the electrodes. It was reported that the recovery rates after separation procedures ranged from 47 to 79 % of the starting cell number and higher recovery rates were obtained with fewer input cells.

An alternative electrode-based DEP method is proposing nDEP-based microwells for single cell patterning using GFP-expressing HeLa cells [6]. This technique offers unique advantages as distinct from the pDEP trapping methods. Unlike other DEP techniques, nDEP microwells do not require a specific buffer for conductivity adjustment; it enables the use of culture media of the cells. Also, by trapping single cells in microwells, cells align in a way that enables constructing and studying neuronal networks and stem cell niches in vitro. These features provide real-life conditions for single-cell studies.

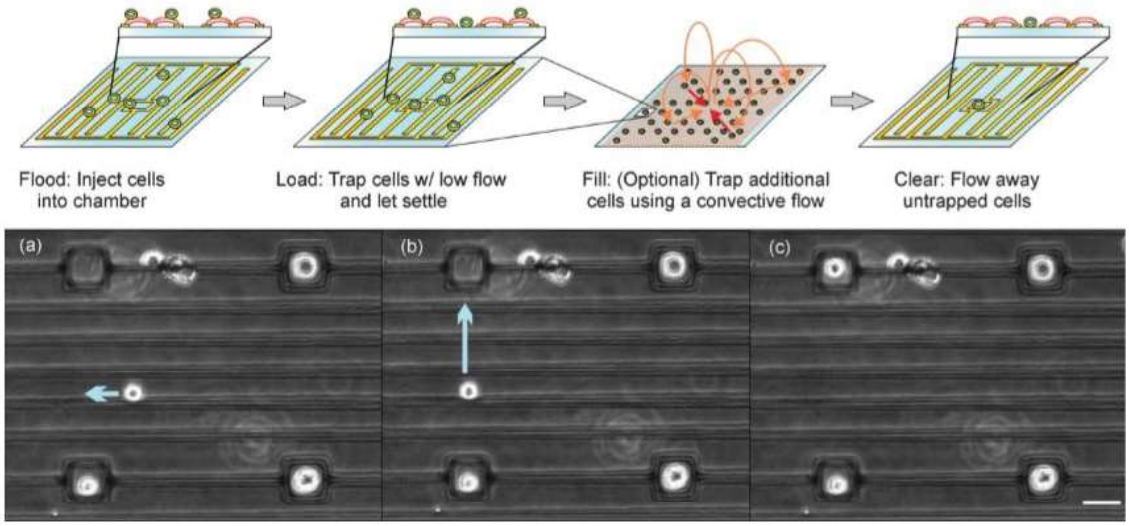

FIGURE 2.7: Schematic of the operating procedure at the top and the real-time images of use of convective flow to pattern cells. Image acquired from [6].

The nDEP microwells were designed as array-like, gold patterned square interdigitated electrodes with an inner square side length of $25\mu m$ and widths of $10\mu m$. Electrode lines were spaced $10\mu m$ away from other lines. The top part of figure 2.7 illustrates the schematic of the operating procedure of the nDEP microwells. After the cells were injected into the chamber with the electrodes on, cells were loaded into traps with very low flow rates. Orange lines in the filling step demonstrate

the motion of the fluid and the red lines show the motion of untrapped cells. The bottom part of the figure demonstrates the trapping of a single-cell with the use of convective flow when the applied electric field was 2.5 Vpp.

Insulator-based dielectrophoresis (iDEP) is another powerful and accepted method in dielectrophoretic separation applications. Studies using insulating post arrays and external electrical field have been expanded, yet the Joule heating is still crucial in many DEP studies. Joule heating is the process where the energy of an electric current is converted into heat as it flows through a resistance. Even though Joule heating can occur in both electrode-based DEP and iDEP, it is more effective in iDEP applications because higher electric potentials are needed for this method. Moreover, due to the external electric field, the temperature gradient can cause bulk fluid forces and consequently fluid motion called electrothermal flow (ET). These unwanted flow circulations might cause clogging at the outlets of the system. Moreover, the temperature gradient could decrease the cell viability [38].

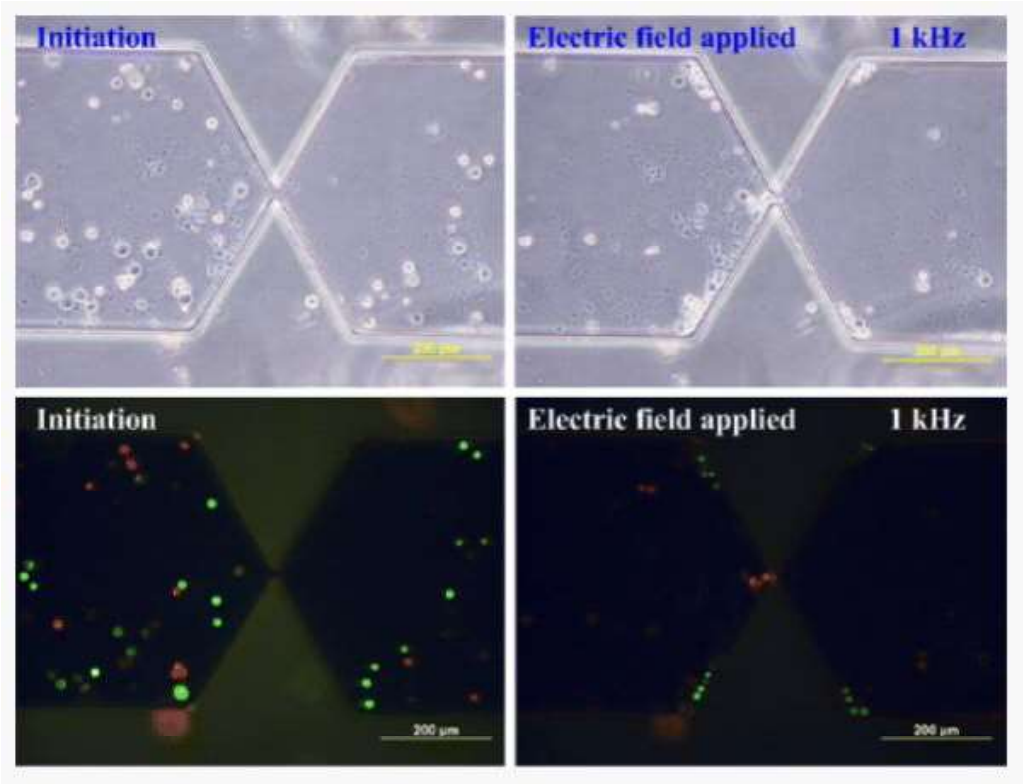

FIGURE 2.8: Real-time images of selective trapping of dead cells at 1 kHz, 3.5×10^4 V/m. The angle of the insulating constriction is 60°. Image acquired from [7].

Figure 2.8 shows an iDEP chip with an open-top structure. The insulators have $70\mu m$ thickness, and the distance between them is $500\mu m$. The spacing of constriction is $20\mu m$ with 60° angle. iDEP chip was used to separate dead HeLa cells from the live ones. To reduce the required voltage, the microelectrodes were deposited on the substrate. Cells were dielectrophoretically characterized under different frequencies, and 1 kHz was chosen as separation frequency because live cells exhibited nDEP while dead cells exhibited pDEP at 1 kHz. Figure 2.8 presents the configuration of live and dead HeLa cells before and after DEP exposure. Even the live and dead cells were separated within the iDEP device, there was no information about flow applied to the system to enrich the live cells [7].

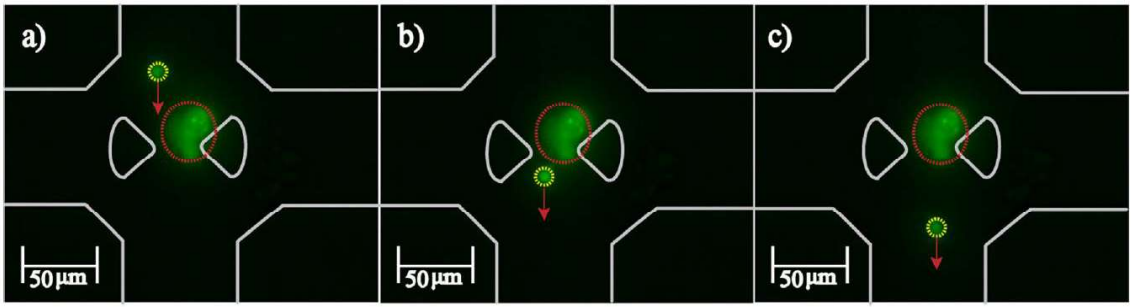

FIGURE 2.9: The real-time images of selective trapping for MCF-7 and PBMCs. Image acquired from [8].

In the study of Bhattacharya *et al.* iDEP was implemented with DC voltage for selective trapping of single MCF-7 breast cancer cells from PBMC and MDA-MB-231 breast cancer cells. Insulating posts of the microfluidic device fabricated with a teardrop shape, which was demonstrated in figure 2.9, to optimize the selectivity of MCF-7 breast cancer cells. PBMC flow through the trapping region when outlet voltage was -50 V and inlet voltage was 50 V. After 2 minutes under DEP exposure, only 68.5 % of the MCF-7 cell population, 51.8 % of the PBMC population and 63.4 % of MDA-MB-231 cell population remained viable. The low viability was due to the high electric field applied to trap MCF-7 cells.

Contactless dielectrophoresis (cDEP) is another DEP method that generates an electric field gradient without having electrodes in contact with the sample fluid. Shafiee et al. presented two different electrode configurations to isolate live human

leukemia cells from dead cells [9]. Metal electrodes were isolated from the main flow channel with a very thin layer of PDMS membrane. 20 μm membrane thickness was appeared to be suitable for cutting the contact while still providing good capacitive coupling of the electric field into the main channel. An observed advantage of this application is reducing electrode lysis and fouling. However, higher voltages were needed to generate a sufficient electric field through the channel in this DEP approach.

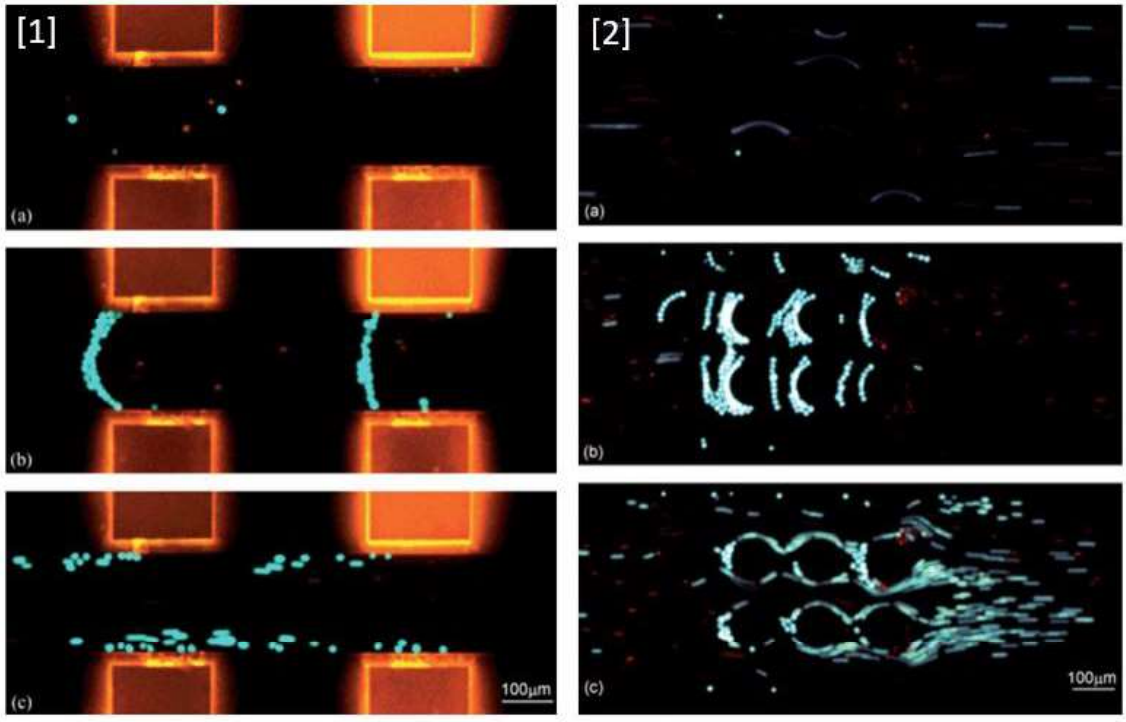

FIGURE 2.10: Snapshots of isolation of live THP-1 cells from the dead ones in two different devices. Image acquired from [9].

Figure 2.10 demonstrates the experimental results of separation of live and dead THP-1 cells in two devices. In device one, square-shaped electrodes were fabricated. 152 kHz, 100 Vrms was applied to trap live cells (blue) with pDEP, while dead cells (red) pass by due to flow. In device two, circular electrodes were used to trap live cells due to pDEP at 500 kHz, 40 Vrms. The trapping efficiency was reported as 89.6% at 0.02 $mL\ h^{-1}$ and 44.8% ($\pm$14.2) at 0.8 $mL\ h^{-1}$. It was also delivered that cell damage due to cell lysis occurred at all frequencies when a 50 Vrms voltage was applied.

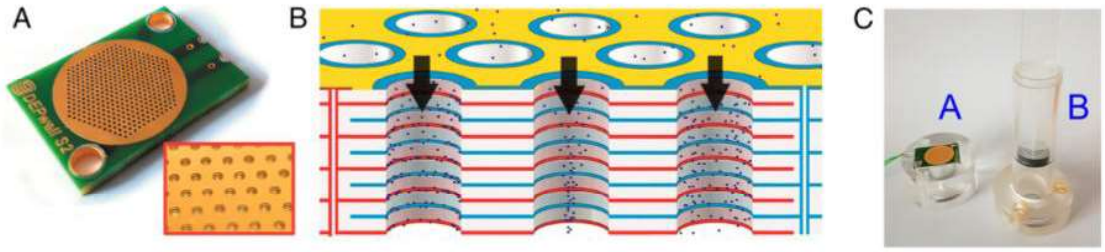

FIGURE 2.11: The cylindrical well formed DEP separation chip. Image acquired from [10].

An interesting and straightforward DEP technique was presented by Faraghat *et al.* offers to preserve cell viability and achieve high-throughput separation using 3D electrodes on a low-cost disposable chip. The device comprised of three main parts; fluidic chip, package and support instruments. The chip consisted of $70\mu m$ thick, 10 layers of circular copper separated by $150\mu m$ thick glass fiber reinforced epoxy (FR4) layers. 397 wells with $400\mu m$ diameter were drilled at the center of the chip. The successful parallelization of the system that demonstrated in figure 2.11 eliminates the risk of bubble formation, which is one the most common cumbersome of the lab-on-a-chip devices. Live/dead yeast; human cancer cells/red blood cells; and rodent fibroblasts/red blood cells separation was conducted. It was reported that cells were enriched with cell recovery of up to 91.3% at over 300,000 cells per second with $> 3\%$ cell loss at 18 Vpp up to 1 MHz frequency.

Carbon electrodes exhibit a wider electrochemical window ($\sim 4.4V$) between oxidation and reduction potentials than platinum or gold electrodes exhibited ($\sim 2.8V$). Their mechanical and electrochemical properties enable generating suitable electric fields with applied high voltages, while not causing electrolysis inside the channel. Islam *et al.* used 3D carbon-electrode DEP for the enrichment of yeast cell populations at increasing flow rates. Figure 2.12 (a) illustrates the yeast cells trapped on the 3D carbon-electrodes at 100 kHz, 20 Vpp and the flow rate was $10\mu l/min$. The trapping efficiency was reported as 100% for the cell concentration $10^2{-}10^4$ $cells/ml$. It was also notified that 3D-electrodes polarize not only the surface of the channel but also the complete bulk of the solution when compared to

more traditional planar devices. In this way, all of the particles inside the channel were addressed, and the trapping efficiency was increased.

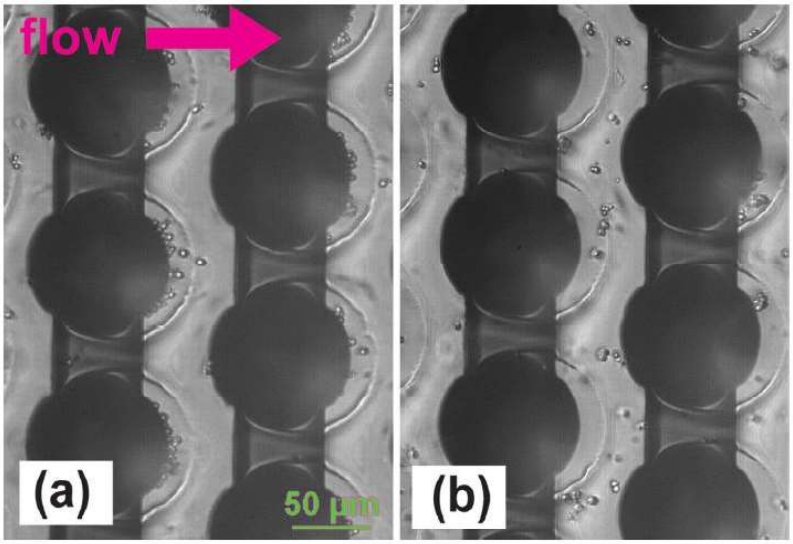

FIGURE 2.12: (a) Yeast cells trapped on the 3D carbon electrodes, (b) not trapped when the carbon electrodes are not polarized. Image acquired from [11].

Dielectrophoresis is accepted and implemented as one of the most promising cell characterization and separation tools. Therefore, a whole range of DEP methods have been developed, and some of these techniques were presented here. As summarized in this review, established devices have been used for the characterization and separation of leukocytes as well as many other bioparticles. However, while resolving some of the problems that were encountered previously, many of these devices faced with new obstacles. Metal electrodes were used to achieve strong DEP forces but ended up decreasing the cell viabilities. Some devices used insulated electrodes to cut the direct interaction with the cells to increase viability, yet they needed high voltages up to hundreds to observe DEP effect. Other devices used reservoirs, which caused cloggings and decreases in separation purities. 3D carbon-electrode DEP device is capable of achieving highly efficient cell separations while preserving the viability of the cells with a fast and accurate manner. In this study, 3D carbon-electrodes were used to efficiently characterize and separate leukocyte subpopulations.

Chapter 3

Materials and Methods

3.1 3D Carbon-Electrode Device Fabrication

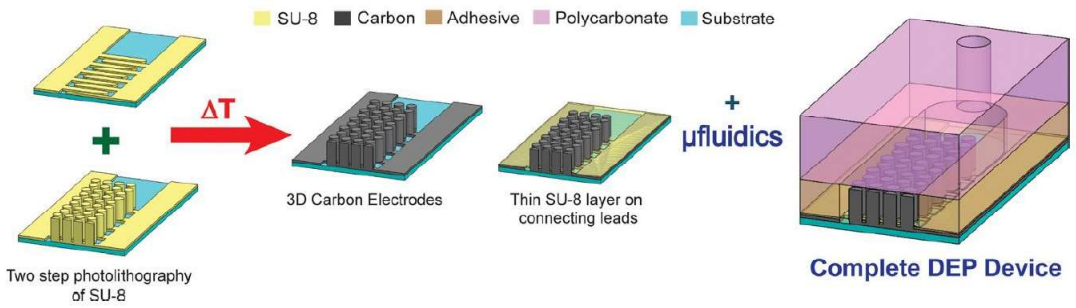

FIGURE 3.1: The fabrication stages of 3D carbon-electrode dielectrophoresis device [11].

The entire fabrication stages of 3D carbon-electrodes has been specified as presented in figure 3.1 in literature [11, 39–42]. In this research, the 3D microelectrodes were produced with a two-step photolithography process of SU-8 (Gersteltec, Pully, Switzerland) on a silicon wafer. Heat treatment was applied with high temperatures to carbonize the microelectrodes in a nitrogen atmosphere. The 3D carbon-DEP device was consisted of more than 3000 electrodes with 100 μm heights and 50 μm diameters. The bottom channel was planarized and connection leads were insulated with a thin layer of SU-8. A channel with 1.8 mm width and 3.2 cm length was

cut from a double-sided pressure sensitive adhesive with $127\mu m$ thickness (PSA, Switchmark 212R, Flexcon, Spencer, MA, USA). Finally, channel was adhered to a drilled polycarbonate, placed around the carbon-electrode array by hand and sealed with a rolling press [11, 14].

3.2 Cell Preparation

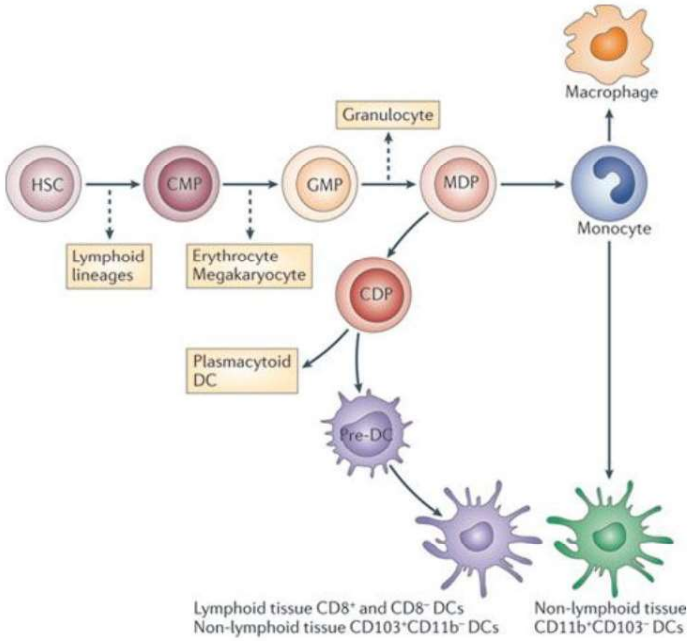

FIGURE 3.2: Transformation process of a monocyte from a haematopoietic stem cell progenitor. Image acquired from [12].

Monocytes are blood circulating leukocytes that originate from hematopoietic stem cells from the adult bone marrow. The hematopoietic stem cells must experience a series of divisions before they are transformed into monocytes as demonstrated in Figure 3.2. Monocytes constitute between 3%-8% of the circulating cell population under usual circumstances, yet their number increases in response to an infection and they can migrate out of the bloodstream to differentiate into macrophages [43, 44].

In this study, the U937 monocyte (the human myeloid leukemia) cell line was obtained from ATCC (American Type Culture Collection, Manassas, VA, USA) and was cultured in a RPMI-1640 complete medium (PAN-Biotech, Aidenbach, Germany) supplemented with 10% fetal bovine serum (FBS; PAN-Biotech, Aidenbach, Germany) and 1% Penicillin-Streptomycin solution (PAN-Biotech, Aidenbach, Germany) under a 5% CO_2 - 95% air atmosphere in a humidified incubator (Nuve, Ankara, Turkey). Before each DEP characterization experiment, cells were spun down at 3000 rpm (MERCK, Darmstadt, Germany) for 5 minutes and resuspended in the low conductive DEP buffer, which was prepared diluting 8.6% sucrose (neoFroxx, Hesse, Germany), 0.3% glucose (Sigma-Aldrich, Darmstadt, Germany) and 0.1% BSA (PAN-Biotech, Aidenbach, Germany) in distilled water. The conductivity of the final suspension was 20 $\mu S/cm$, measured by a conductivity meter (Cambridge Scientific Products, Watertown, MA, USA).

For the induction of cell differentiation, the U937 monocytes ($2.5\times10^5 cells/ml$) were seeded in a complete medium with 2.5 μl of 10 ng/ml phorbol myristate acetate (PMA)/DMSO (PAN-Biotech, Aidenbach, Germany) solution for 5 days. In day 3 and 4 nonattached cells were removed by aspiration, and the adherent cells were washed with a complete medium. In day 5 after aspiration of the nonattached cells, differentiated macrophages were washed first with PBS (PAN-Biotech, Aidenbach, Germany) and then incubated for 10 minutes with 1 ml pre-warmed trypsin solution (PAN-Biotech, Aidenbach, Germany). Detached macrophages were spun down at 3000 rpm for 5 minutes to remove any residual culture media and resuspended in the low conductive DEP buffer for DEP characterization experiments. The cell number of monocytes and macrophages were arranged to $1 \times 10^6 cells/ml$ using a hemocytometer (Marienfeld-Superior, Lauda-Knigshofen, Germany).

For the live and dead cell separation experiments cells were obtained from the same culture to eliminate the risk of physical environment variations when they grow in different flasks. The live and dead cells were distinguished using the Trypan blue dye (Sigma-Aldrich). The number of cells was adjusted to $1 \times 10^6 cells/ml$ with a 1:1 cell ratio.

3.3 Immunophenotyping

The CellTracker Green CMFDA and CellTracker Red CMTPX dyes (Thermo Fisher Scientific, New Hampshire, United States) were used to prepare a 1 μM staining solution in a serum free RPMI-1640 medium. While the U937 monocytes were incubated with the CellTracker Green CMFDA dye, the differentiated macrophages were incubated with CellTracker Red CMTPX dye for 30 minutes. After incubation, the stained cells were spun down at 3000 rpm for 5 minutes to remove any residual dye in the culture media and resuspended in the low conductive DEP buffer. The cells were incubated for 10 additional minutes in case of extra dye release into the DEP buffer and washed again in the DEP buffer for the separation experiment. The number of cells was adjusted to $1 \times 10^6 cells/ml$ with a 1:1 cell ratio for monocyte-macrophage separation experiments.

Immunophenotyping of U937 monocytes and differentiated macrophages was performed on a BD LSRFortessa FACS analyzer (BD Biosciences, Franklin Lakes, NJ, USA). The green fluorescence of CellTracker Green was then detected with the FACS analyzer at FITC-A channel using excitation at 492 nm, while the red fluorescence of CellTracker Red was detected at PE-Texas Red-A using excitation at 577 nm. The immunophenotypic patterns were analyzed using FlowJo v10 software (TreeStar, Inc., OR, USA).

3.4 Image Acquisition and Analysis

The images were acquired using a Nikon Eclipse upright optical microscope (Nikon Instruments Inc., Melville, NY, USA) with 10X objective during the characterization experiments. ImageJ software was used to convert acquired image sequences into movies to analyze the dielectrophoretic behavior of the cells with changing frequencies. Every image displays the positions of the cells for a given frequency. The locations of the cells were ranked from the strong pDEP areas (3) to the strong nDEP areas (-3) as presented in Figure 3.3. While tracking each cell separately, the positions of single cells were determined as strong pDEP (3), pDEP (2), weak pDEP

(1), crossover (0), weak nDEP (-1), DEP (-2) and strong nDEP (-3). The standard deviations of the dielectrophoretic responses for each frequency were calculated using the Prism software.

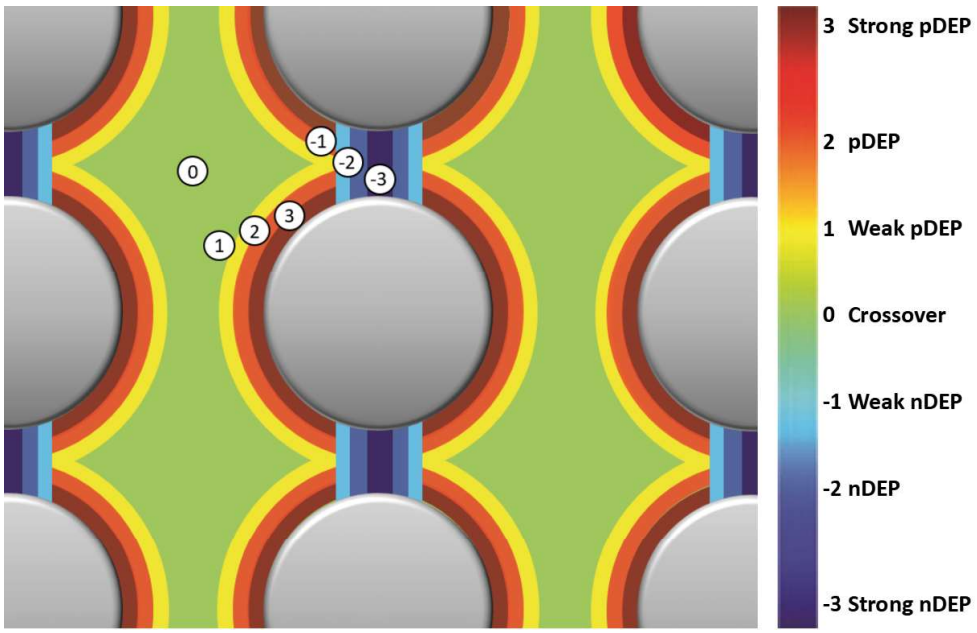

FIGURE 3.3: The schematic diagram for the image analysis on the 3D carbon electrode microchip that represents the DEP regions.

3.5 Experimental Setup and Procedure

The experimental setup, presented in Figure 3.4.A, has a function generator to generate an electric field (GW Instek, New Taipei City, Taiwan), an upright microscope (Nikon Instruments Inc., Melville, NY, USA) to monitor the cells, a computer (Hewlett-Packard Company, Palo Alto, CA, USA) to record sequential images during the experiments, a programmable syringe pump (Model: NE-1000, New Era Pump Systems Inc, Farmingdale, NY, USA) to flow the cells and the DEP buffer in a controlled manner, and the 3D carbon-DEP device. To create reservoirs, two 20-200 μl pipette tips (Eppendorf, Hamburg, Germany) were inserted at the inlet and outlet of the microchannel. The tygon tubings (Cole-Parmer, Vernon Hills, IL, USA) were connected the syringe to the microchannels of the 3D carbon-DEP device.

A

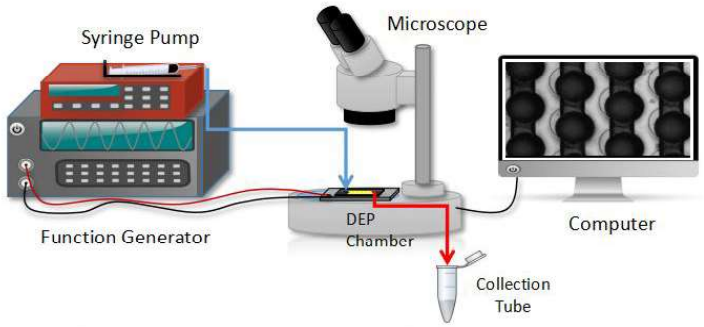

B

Time (min)	Fraction	E field	Inlet tubing	Chip	Outlet tubing		
0	0	OFF					
0-5	1	ON					
5-10	2	ON					
10-20	3	ON					
20-40	4	ON					

FIGURE 3.4: Schematic of the process of separation of U937 monocytes and macrophages using 3D carbon-DEP device. Color coding: blue; mixed cell suspension of monocytes and macrophages, yellow; trapped monocytes in the electrode array, red; macrophages at the outlet tubing.

The crossover frequency experiments were performed to characterize the dielectrophoretic responses of monocytes and macrophages and to decide the required separation frequency. Prior to the experiments, the 3D carbon-DEP device was sterilized with flowing 70% Ethanol and then DI water with a syringe pump. DEP buffer was sent to fill the chip, and all the bubbles were removed. Subsequently, both monocytes and macrophages were prepared separately as explained above and in turn 40 μl cell suspension was sent onto the chip with a 10 $\mu l/min$ flow rate. After the cells reached to the carbon-electrode regions, the flow was stopped and the cells were settled for 30 seconds. 10 Vpp bias with frequencies ranging from 1 kHz to 20 MHz was applied to the 3D carbon-DEP device using a function generator. The cells were then collected inside an Eppendorf tube for further viability assays.

After recording the crossover frequency experiments, the images were analyzed, and 30 kHz was selected as the separation frequency. The U937 monocytes and macrophages were stained as explained in Section 3.3 and mixed at a 1:1 ratio. Figure 3.4.B demonstrates the process of the separation experiments. The first

column shows time (minutes), the second column shows collected fractions by time, and the third column shows electric field signal. The electric field was off at the beginning of the experiment. The monocytes and macrophages were loaded onto the chip using a 10 $\mu l/min$ flow rate. After they reached the region of the carbon electrodes, the flow was stopped and made the cells settle. When the electric field was 30 kHz, 10 Vpp, the U937 monocytes exhibited pDEP, and were trapped at the high electric field regions. Meanwhile the majority of the macrophages remained at the crossover regions. Using the 1 $\mu l/min$ flow rate, the drag force caused the macrophages to flow away from the 3D carbon-DEP chip for 40 minutes and the separated macrophages were obtained at fraction 4. During this 20 minute fraction, 20 μl cells were collected inside a collection tube for further flow cytometry analysis.

For the live and dead cell separation experiments, the signal with 20 Vpp and 300 kHz was applied for the cells in the 3D carbon-DEP device using the function generator. When the electric field was 20 Vpp, due to the selective DEP forces the live cells exhibited strong pDEP while the dead cells remained unresponsive. Using the 1 $\mu l/min$ flow rate, it was allowed the drag force discard the dead cells from the 3D carbon-DEP chip. The dead cells were also collected inside a collection tube for further confirmation. When all the dead cells were removed, the electric field was turned off, and the live cells were flown and collected for further viability tests.

Chapter 4

Dielectrophoretic Characterization of Leukocytes

Dielectrophoretic characterization of cell subpopulations is one of the essential steps for the achievement of high-throughput cell separation. This can be accomplished by determining the specific crossover frequency of cells as signatures. In this study, the dielectrophoretic characterization experiments were conducted using 3D carbon-electrode DEP device to determine the crossover frequency of each cell type.

In this chapter, results of dielectrophoretic characterization experiments of U937 monocytes, U937 monocyte differentiated macrophages, dead leukocytes and fluorescent dyes will be presented. Also, a numerical study that investigated the dielectrophoretic responses of several blood cells will be demonstrated to give an overview of DEP responses of different cell types and to compare the experimental outcomes with the numerical results.

4.1 Monocyte Characterization

In this section, the dielectrophoretic response of U937 monocytes is investigated. U937 monocytes were prepared as explained in Section 3.2 and the dielectrophoretic characterization experiments were performed as described in Section 3.5. The images of the cells were acquired with 1 fps frame rate using Nikon Eclipse upright optical microscope (Nikon Instruments Inc., Melville, NY, USA) with 10X objective. The obtained images were manually analyzed using ImageJ as represented in Section 3.4.

Figure 4.1 demonstrates the dielectrophoretic response of U937 monocytes under 10 Vpp bias. The figure illustrates the response of 50 cells for each frequency from 8 kHz to 30 kHz with error bars. The results indicate that monocytes exhibit both negative dielectrophoresis (nDEP) and positive dielectrophoresis (pDEP) behaviors and have a crossover frequency at 18 kHz.

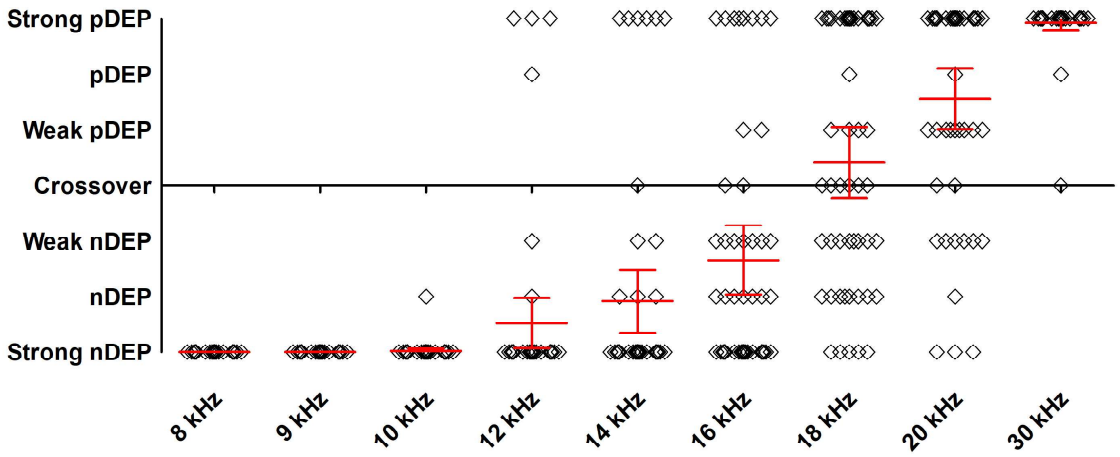

FIGURE 4.1: DEP response of U937 monocyte [13].

The real-time images of U937 monocytes under 10 Vpp bias at different frequencies are demonstrated in Figure 4.2. The DEP regions of 3D carbon-electrode chip are detailed earlier in Section 3.4. Figure 4.2.A. shows the positions of cells under nDEP forces. The cells were at the planar connection leads, which were insulated with a thin layer of SU-8, due to the repulsion of carbon-electrodes. At the

crossover frequency (18 kHz), cells were feeling almost zero force acting on them, so they started to release from the connection leads as demonstrated in Figure 4.2.B. When the frequency was increased, the cells were captured by electrodes, and the pearl chains occurred due to dipole-dipole attractions between the cells as presented in Figure 4.2.C. In this position, the cells were under pDEP.

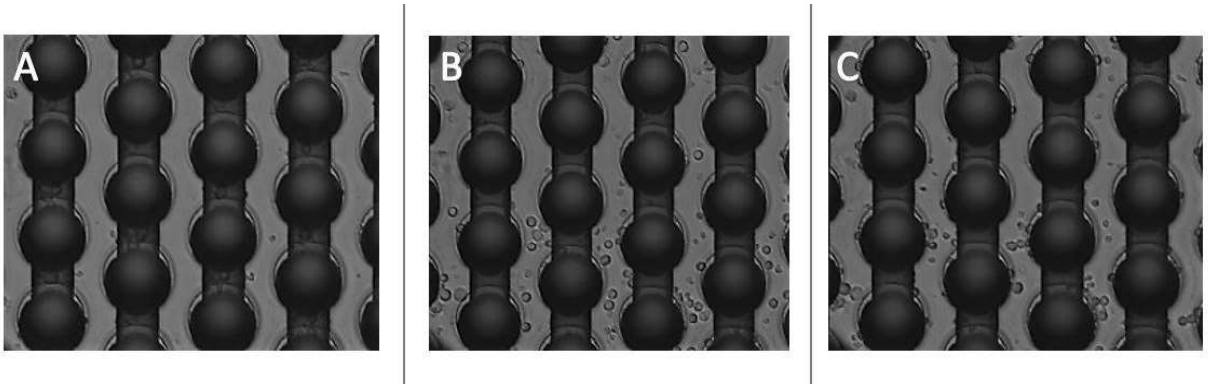

FIGURE 4.2: The real time images of U937 monocytes at different frequencies.

The frequency scanning process is reversible that means; if the frequency started to be decreased when cells were at pDEP regions, they would start to migrate through crossover regions and then to the nDEP regions.

4.2 Macrophage Characterization

In this section, the dielectrophoretic response of U937 monocyte differentiated macrophages is investigated. The macrophages were prepared as explained in Section 3.2 and the dielectrophoretic characterization experiments were performed as described in Section 3.5. The images of the cells were acquired with 1 fps frame rate. The obtained images were manually analyzed using ImageJ as represented in Section 3.4.

Figure 4.3 demonstrates the dielectrophoretic response of the macrophages under 10 Vpp bias. The figure illustrates the response of 50 cells for each frequency from 8 kHz to 30 kHz with error bars. The results indicate that macrophages exhibit both negative dielectrophoresis (nDEP) and positive dielectrophoresis (pDEP) behaviors like U937 monocytes, yet their crossover frequency is 30 kHz.

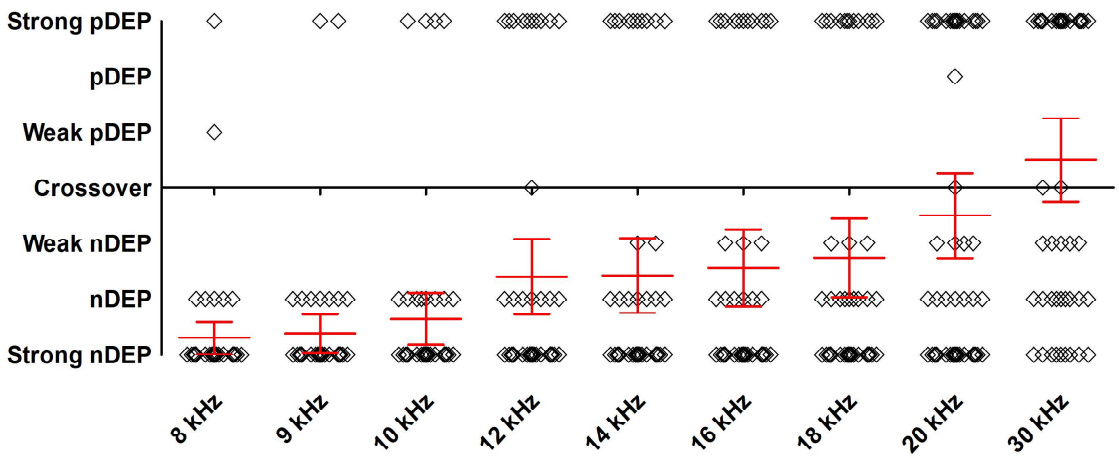

FIGURE 4.3: DEP response of U937 monocyte differentiated macrophages.

At 30 kHz frequency, U937 monocytes were at strong pDEP regions as demonstrated in Figure 4.1. This specific DEP response difference between monocytes and macrophages is very crucial for cell separation because carbon-electrodes will strongly capture monocytes while the macrophages will not be affected by the electric field at 30 kHz and will be able to wash away by a drag force. The frequency scanning process is also reversible for macrophages as well meaning that; if the frequency started to be decreased when cells were at pDEP regions, they would start to migrate through crossover regions and then to the nDEP regions.

4.3 Characterization of Dead Leukocytes

In this section, the dielectrophoretic response of dead leukocytes is investigated. The content which is presented in this section has been published in [14]. The dielectrophoretic forces those dead cells experienced were not distinct during the dead leukocyte characterization experiments. However, our experimental observations showed that the dead cells moved towards the weak nDEP regions or were not affected by the DEP forces and stayed around the crossover regions at every frequency. The reason for this response is that the dead cells with an impaired membrane polarize differently than live cells under the applied electric field [45, 46].

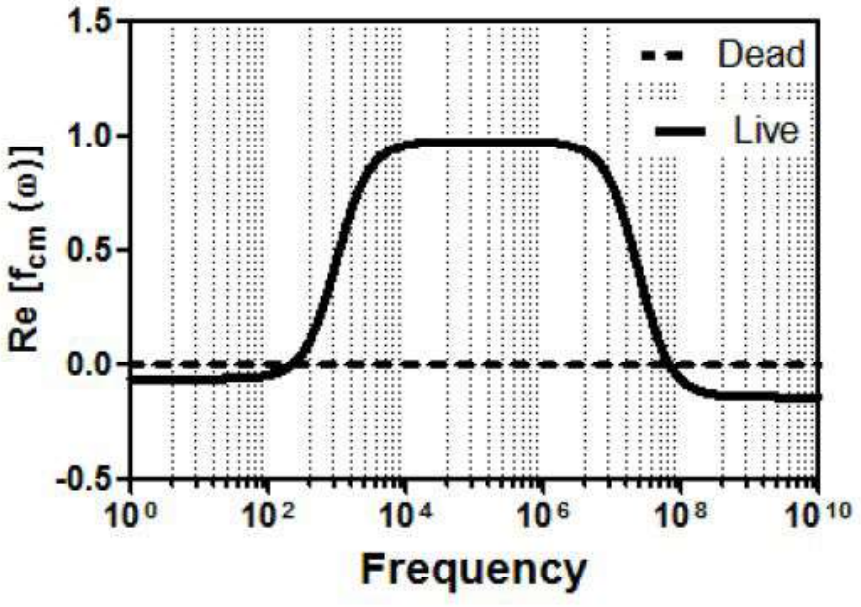

FIGURE 4.4: Numerical characterization of the live and dead U937 monocytes[14].

The behavior of live and dead cells was simulated using Matlab (Version R2016a, The MathWorks Inc., Natick, MA, USA) for numerical confirmation because the experimental results for dead cells were not very clear. The cell parameters were taken from [15] for U937 monocytes. The dielectrophoretic responses of live and dead cells for the frequency ranging from 1 Hz - 1010 Hz are demonstrated in Figure 4.4. Both live and dead cells had 7 nm membrane thickness and 12.50 ε_0 membrane permittivity. For the live cells, the diameter was 23 μm, the cytoplasm conductivity was 0.5 S/m, the cytoplasm permittivity was 50 ε_0 and the membrane conductivity was 10^6 S/m. For the dead cells, the diameter was 22 μm, the cytoplasm conductivity was 0.002 S/m and the cytoplasm permittivity was 80 ε_0. The membrane conductivity was taken as 0.01 S/m, because it was reported that membrane conductivity increases by 10^4 fold when a cell is dead [47]. Also, the conductivity of the medium was taken as 0.002 S/m and the permittivity of the medium was $80\varepsilon_0$. ε_0: 8.85×10^{-12} F/m in this calculations.

4.4 Characterization of Fluorescent Dyes

In this section, the dielectrophoretic characterization of U937 monocytes stained with commercially available fluorescent dyes in the stationary liquid is presented. The content which is presented in this section has been published in [13]. The cells were prepared as explained in Section 3.2 and stained as in Section 3.3. The dielectrophoretic characterization experiments were performed as described in Section 3.5. The images of the cells were acquired with 1 fps frame rate. After the DEP exposure, the cells were collected from the device into a collection tube and analyzed as explained in Section 3.4.

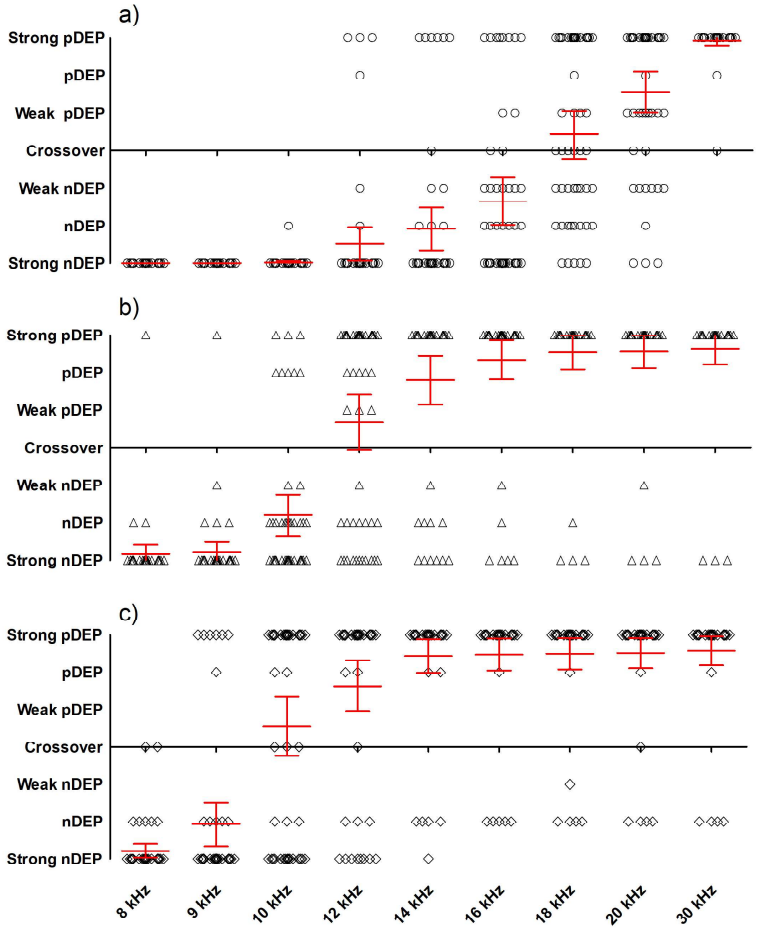

FIGURE 4.5: DEP responses of monocytes. (a) Unlabeled monocytes. Monocytes stained with (b) CellTracker Red, (c) CellTracker Green [13].

Figure 4.5 demonstrates the obtained dielectrophoretic behavior of the label-free U937 monocytes and the monocytes stained with CellTracker Red and CellTracker Green dyes. 50 cells were tracked from 1 kHz to 30 kHz under 10 Vpp bias at single-cell resolution. The red lines demonstrate the mean and standard deviation for the cells at each frequency. As shown in figure 4.6, there is a slight shift in the crossover frequencies of the cells when they were stained with membrane-permeant reactive tracers.

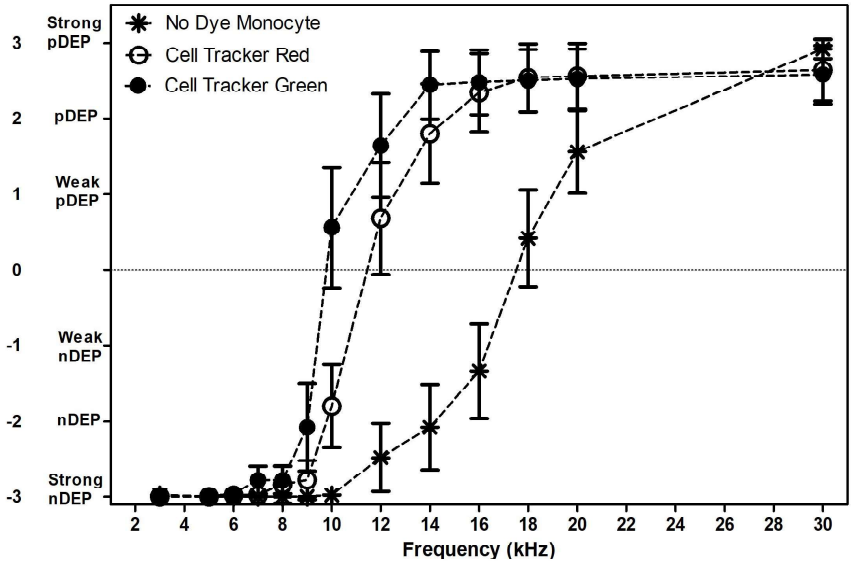

FIGURE 4.6: DEP response of monocytes stained with CellTracker Red (white circles), CellTracker Green (black circles), and DEP response of unlabeled monocytes (star)[13].

4.5 Numerical Methods for Characterization of Leukocytes and RBCs

In this section, numerical analysis for dielectrophoretic characterization of red blood cells, T-lymphocytes, B-lymphocytes and monocytes is presented to give an overview of DEP responses of different cell types. The content which is presented in this section has been published in [15]. The single-shell spherical cell model, detailed

in Section 2.1.2, was used for numerical characterization of blood cell subpopulations [48]. Since, different subpopulations display distinct membrane morphologies, the membrane folding factor (ϕ), introduced by Gascoyne and Shim, was used to implement membrane differences to the dielectrophoretic force. This enables the separation of cancer cells from the blood because their membrane folding factor greater than the other type of blood cell populations [49].

Membrane folding factor is demonstrated in equation 4.1 and the complex effective permittivity after adding ϕ to the equation is shown in equation 4.2.

$$\phi = \frac{A}{4\pi r^2} \tag{4.1}$$

$$\varepsilon^*_{eff} = \varepsilon^*_{mem} \frac{(\frac{r\phi}{r\phi - d})^3 + 2\frac{\varepsilon^*_{int} - \varepsilon^*_{mem}}{\varepsilon^*_{int} + 2\varepsilon^*_{mem}}}{(\frac{r\phi}{r\phi - d})^3 - \frac{\varepsilon^*_{int} - \varepsilon^*_{mem}}{\varepsilon^*_{int} + 2\varepsilon^*_{mem}}} \tag{4.2}$$

Table 4.1 demonstrates the dielectric parameters (radius, medium conductivity-permittivity, membrane conductivity-permittivity of the cell, cytoplasm conductivity-permittivity of the cell, the measured surface area of the cell and calculated membrane folding factor) of RBC, T-cell, B-cell and U937 Monocytes from literature. The dielectrophoretic responses of cell subpopulations with and without membrane features were calculated using MATLAB.

Figure 4.7 shows the DEP responses of T-cell, B-cell, RBC, and U937 monocytes using single-shell model assuming that the membrane of these cells is homogeneous. The crossover frequencies of cells differ under the same medium conditions, because of their intrinsic dielectric properties as presented in table 4.1. T-cells and B-cells only exhibit pDEP while RBCs and U97 monocytes exhibit both nDEP and pDEP.

TABLE 4.1: Dielectric parameters of leukocytes and RBCs. Table acquired from [15].

Dielectric parameters (Symbol, unit)	**RBC**	**T-cell**	**B-cell**	**U937 Monocyte**
Radius (r, μm)	2.8	3.29	3.29	7
Membrane thickness (d, nm)	4.5	7.5	7.5	7
Medium conductivity (σ_m, S/m)	0.01	0.01	0.01	0.01
Medium permittivity (ε_m, F/m)	$80\varepsilon_0$	$80\varepsilon_0$	$80\varepsilon_0$	$80\varepsilon_0$
Membrane conductivity (σ_{mem}, S/m)	10^{-6}	2.7×10^{-5}	5.6×10^{-5}	10^{-6}
Membrane permittivity (ε_{mem}, F/m)	$4.44\varepsilon_0$	$8.89\varepsilon_0$	$10.67\varepsilon_0$	$12.5\varepsilon_0$
Cytoplasm conductivity (σ_{int}, S/m)	0.31	0.65	0.73	0.5
Cytoplasm permittivity (ε_{int}, F/m)	$59\varepsilon_0$	$103.9\varepsilon_0$	$154.4\varepsilon_0$	$50\varepsilon_0$
Measured surface area of the cells (A, μm^2)	–	–	265	280
Membrane folding factor (Φ)	1	1.22	1.94	0.45

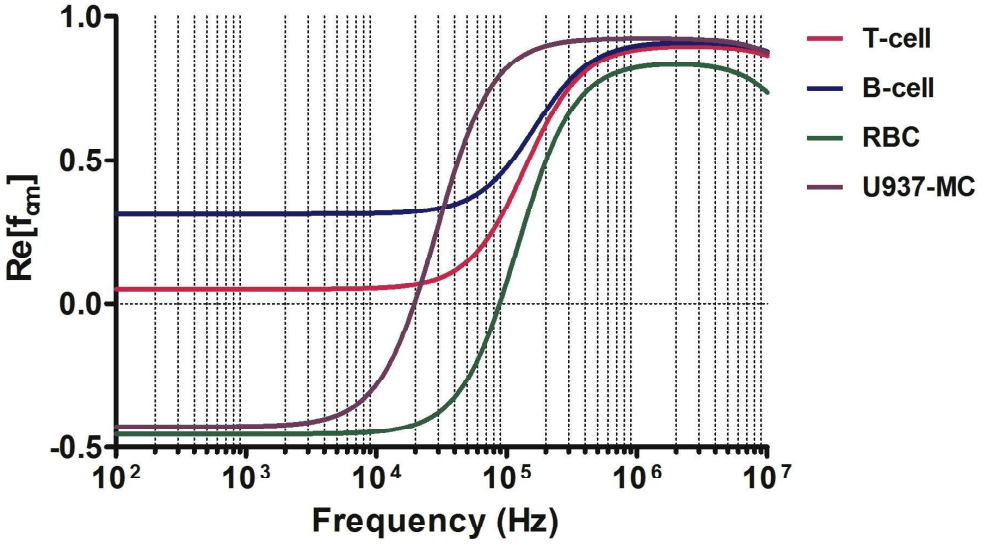

FIGURE 4.7: Re[fcm] vs. applied frequency graph of T-cell, B-cell, RBC and U937-MC [15].

Figure 4.8 presents the DEP responses of T-cell, B-cell, RBC, and U937 monocytes when measured membrane surfaces or membrane folding factors are implemented in our MATLAB code. The overall DEP trend remained the same as well as the crossover frequency of RBC (88.35 kHz), while the crossover frequency of U937 monocytes increased 44 kHz. T-cells with folding-factor 1.22 and B-cells with folding-factor 1.94 still exhibit only pDEP behavior, yet their overall DEP-response curves are shifted as compared in table 4.2.

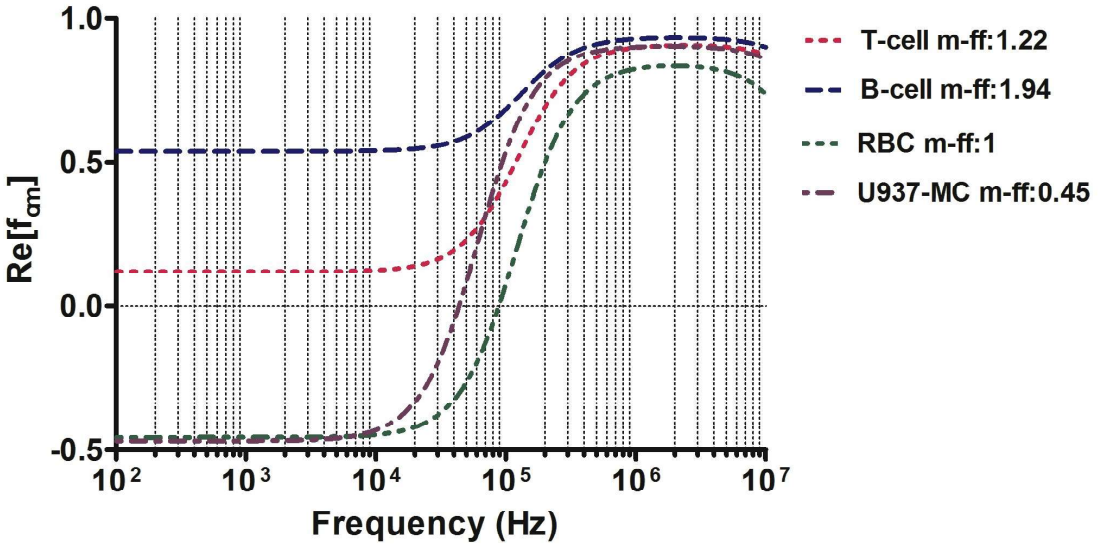

FIGURE 4.8: Re[fcm] including membrane features vs. applied frequency graph of T-cell, B-cell, RBC and U937-MC [15].

TABLE 4.2: Crossover frequencies and dielectric responses of leukocytes and RBCs. Table acquired from [15].

Membrane morphology	**RBC**	**T-cell**	**B-cell**	**U937 Monocyte**
Smooth	88.35 kHz	pDEP	pDEP	19.59 kHz
Membrane features	88.35 kHz	pDEP	pDEP	44 kHz

4.6 Discussion

Studies of leukocyte subpopulations often demand their separation and purification. As previously studied and presented in figure 4.9, dielectrophoretic responses of leukocyte subpopulations are quite close to each other. Therefore, the separation of these cell types is relatively challenging. However, it still required for several hematological tests and for identification of infection, inflammation, allergies, and leukemia. The 3D carbon-DEP method enabled a rapid and efficient characterization of live and dead U937 monocytes and macrophages. The DEP forces were observed distinctly, and high trapping efficiencies indicate that high throughput separations are possible with this device.

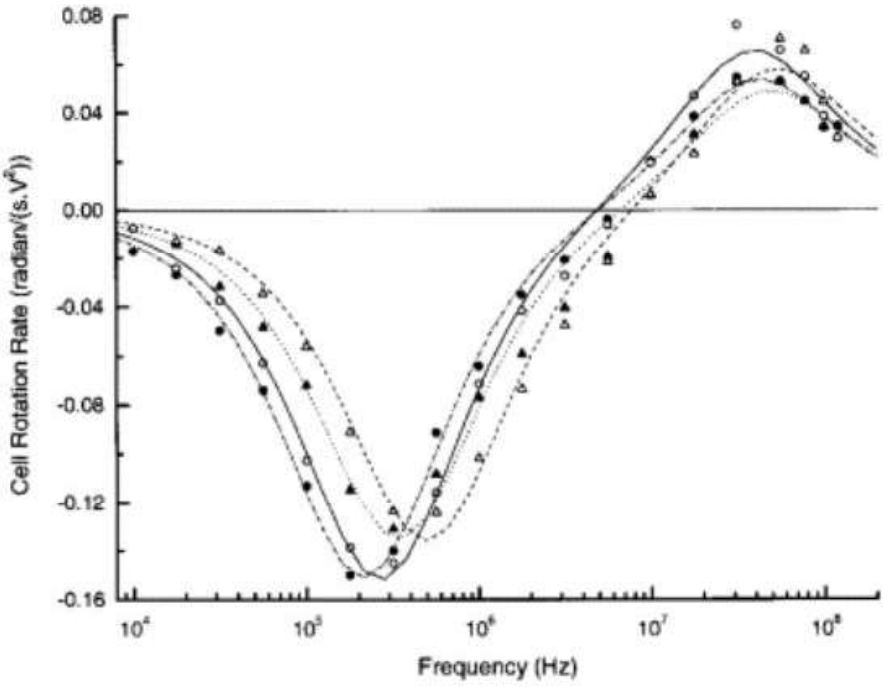

FIGURE 4.9: Typical ROT spectra for human peripheral blood T-lymphocytes (△), B-lymphocytes (▲), monocytes (•), and granulocytes (○) in an isotonic sucrose suspension of conductivity 56 mS/m. Image acquired from [16].

Another required investigation was observing the effects of commercially available fluorescent dyes on DEP responses of the cells. Fluorescent dyes have been widely used for cell labeling in many applications of medicine and biology. They are

highly efficient in monitoring cell movement and migration and quantifying proliferation. Most of these dyes are capable of penetrating through the cell membrane, passing into the cytoplasm, and being permeant. However, their effects on the permittivity and conductivity of the cell membrane and cytoplasm have not been examined previously. In the study presented in Section 4.4, the effects of CellTracker Green and CellTracker Red dyes on dielectrophoretic responses of cells were observed. After staining, a slight shift in the crossover frequencies of cells was detected. This minor variation might be negligible for many applications. However, it is considerable for the dielectrophoretic separation of cells that exhibit very close dielectrophoretic responses at single-cell resolution such as leukocytes.

Mathematical models and numerical solutions provide insight into dielectrophoretic investigations of the blood cells. Therefore, these models need to be improved to provide the most realistic form of cell modeling. The proposed model in Section 4.5 incorporates the membrane features of a cell considering that leukocytes and RBCs have different intrinsic and membrane properties. The results showed that the membrane morphology alters the crossover frequencies of U937 monocytes and RBCs, while affecting the magnitude of pDEP responses of T-cells and B-cells.

Chapter 5

Dielectrophoretic Separation of Leukocytes

The high-throughput separation of leukocyte subpopulations is vital in treatment and diagnosis that demand high-quality and accuracy. Achieving efficient separation while preserving the phenotype, genotype and viability of cells are the primary objectives during this process. In this study, leukocyte subpopulations were separated using 3D carbon-electrode DEP device. The crossover frequencies of cell subpopulations that were discovered in the course of cell characterization experiments were used as signature parameters.

In this chapter, results of dielectrophoretic separation experiments of live-dead monocytes, live-dead macrophages and U937 monocyte-macrophages will be presented. Separation efficiency related to the advantages of the 3D carbon-DEP device will be discussed.

5.1 Live - Dead Monocyte Separation

The results of the dielectrophoretic characterization experiments of live and dead monocytes were presented in Section 4.1 and 4.3 respectively. The live U937 monocytes exhibited both nDEP and pDEP behaviors with a crossover frequency at 18 kHz under 10 Vpp bias. On the other hand, dead monocytes displayed either very weak nDEP behavior or not affected by the electric field during the characterization experiments. The forces acting on the dead cells were not sufficient for experimental observation. Besides, the numerical characterization of dead leukocytes proved that the nonviable cells do not feel the DEP force. Conclusively, live cells must be trapped by the strong pDEP forces at the electrodes to be efficiently separated from dead cells. In this way, dead cells, which were not captured by the electric field, will be washed away with a given flow.

Live and dead monocytes were prepared as explained in Section 3.2 and their numbers were adjusted to $1 \times 10^6 cells/ml$ with a 1:1 cell ratio. 20 Vpp, 300 kHz was applied to capture the live cells with a strong pDEP to increase the performance of the separation. 1, 3, 5, 7 and 10 $\mu l/min$ flow rates were applied to determine the most suitable flow rate for the highest separation efficiency. Figure 5.1 demonstrates the removal efficiency (%) of dead cells from the microenvironment with changing flow rates. It was determined by counting the live and dead cells inside the collection tube.

40 μl cell suspension was introduced into the channel. The live cells were concentrated at the pDEP regions applying 300 kHz, 20 Vpp electric-field for 40 min, while the dead cells were removed using the 1 $\mu l/min$ flow rate. The percentage of the live and dead monocytes for pre- and post-DEP separation was demonstrated in figure 5.2. The separation efficiency of live monocytes from the mix cell population was 90.73 %. The Students unpaired t-test (two-tailed) was applied to test the significance of the results using the GraphPad Prism software. The percentage of initial and enriched live monocytes gave $p < 0.0001$ (***) significancy. $P-values < 0.05$ were considered significant [14].

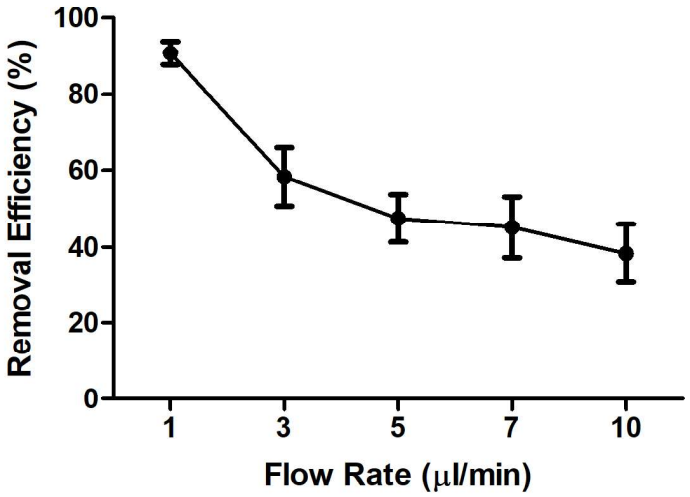

FIGURE 5.1: Removal efficiency (%) of dead cells with changing flow rates ($\mu l/min$) [14].

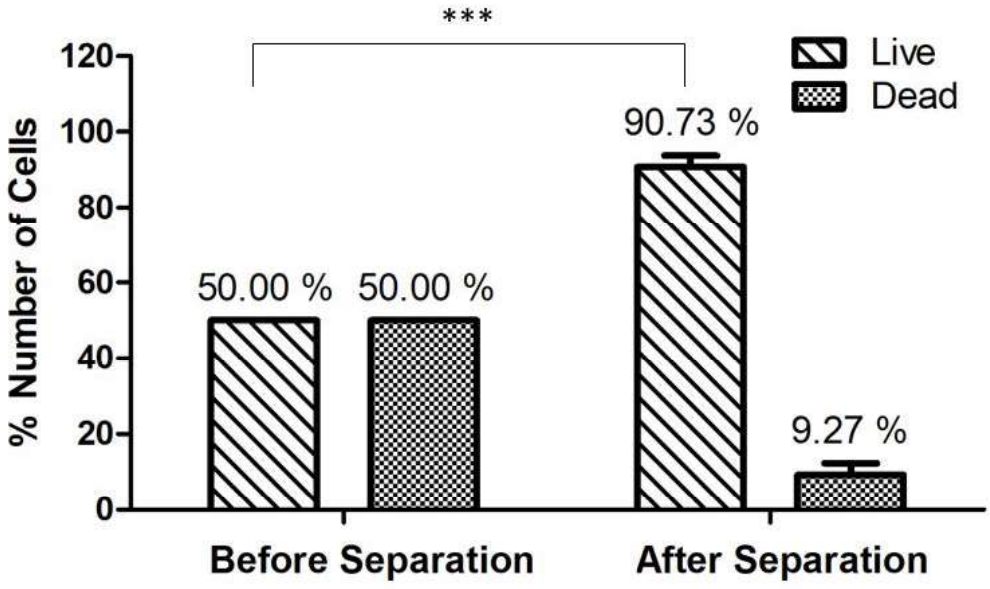

FIGURE 5.2: Separation of the live and dead U937 monocytes using 3D carbon-DEP chip [14].

5.2 Live - Dead Macrophage Separation

Live-dead macrophage separation experiments were conducted using the same conditions and procedures precisely as live-dead monocyte separation experiments as explained in Section 5.1. The separation efficiency of live macrophages from the mix cell population was 93.15 % with $p < 0.0001$ (***) significancy.

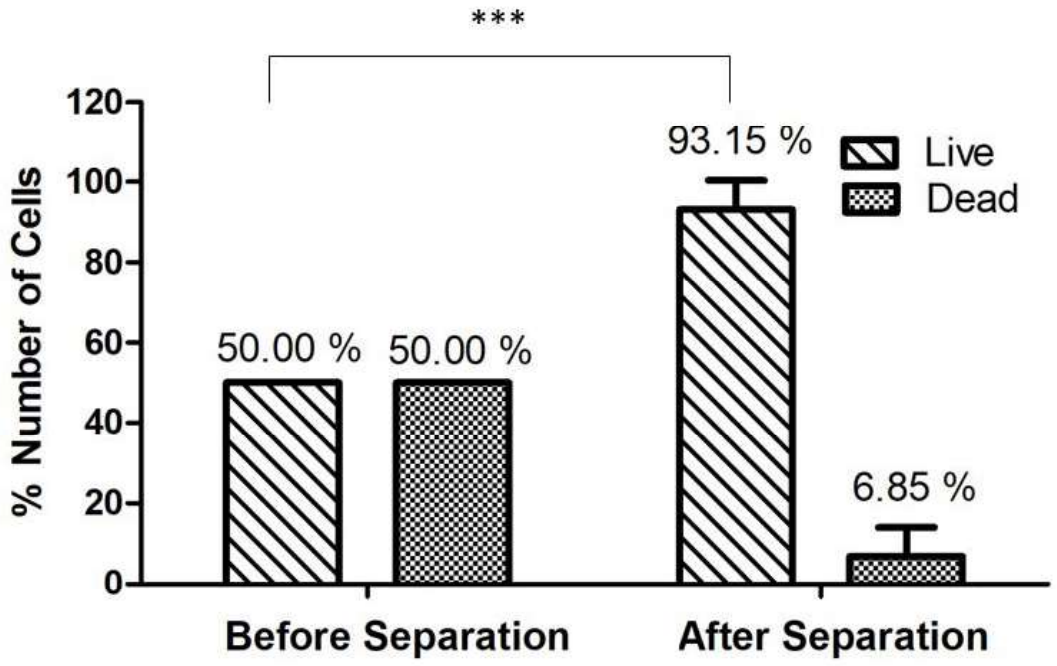

FIGURE 5.3: Separation of the live and dead macrophages using 3D carbon-DEP chip.

5.3 Monocyte - Macrophage Separation

Dielectrophoretic characterization experiments of U937 monocytes and monocyte differentiated macrophages were performed as explained in Section 3.5. The results indicated that monocytes and macrophages exhibit both nDEP and pDEP behaviors, but their crossover frequencies are different from each other as presented in figure 5.4. While the crossover frequency of monocytes is around 18 kHz, the

crossover frequency of the macrophages was 30 kHz under 10 VPP bias. At each frequency, cells from each type displayed variations in their dielectrophoretic behavior, reflecting intrinsic inhomogeneities in the cell dielectrophoretic responses. These inhomogeneities were expected as it is known that monocytes and macrophages are heterogeneous in the peripheral circulation, vary in size and have different degrees of granularity.

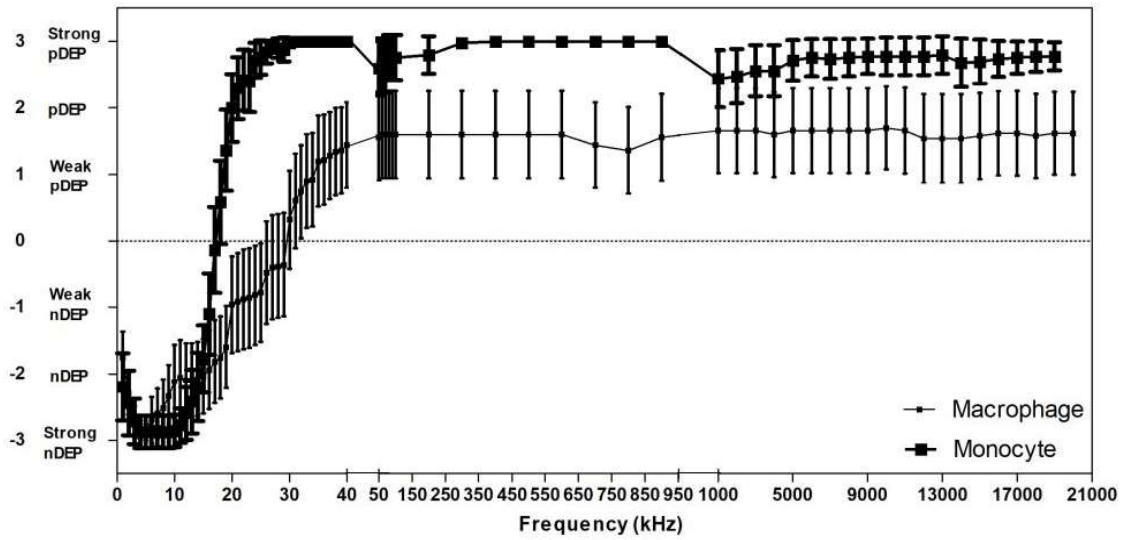

FIGURE 5.4: DEP responses of U937 monocytes and macrophages.

$40\mu l$ cell suspensions of monocytes (stained with CellTracker Green) and macrophages (stained with CellTracker Red) were introduced into the channel. U937 monocytes were concentrated at the pDEP regions applying 30 kHz, 10 Vpp electric-field for 40 min. After on-chip separation, macrophages at crossover regions were removed by washing the array with $1\mu l/min$ flow rate. Monocytes on the 3D carbon-electrodes were collected by the fluidic flow after the voltage was turned off.

The separation efficiency of U937 monocytes and macrophages were tested with flow cytometry as described in Section 3.3. Figure 5.5 is a representative scattergram of flow cytometry analysis. Monocyte and macrophage populations were gated to identify cell percentages after DEP separation. 5 independent experiment were conducted, and the results of these experiments were presented as in figure 5.6. The separation efficiency of U937 monocytes from macrophages was 69.43 %. This

percentage indicates the number of harvested cells after the removal of macrophages from the 3D carbon-DEP device. The lost percentage represents the events (cells) that were left outside the scattergram gates as in figure 5.5.

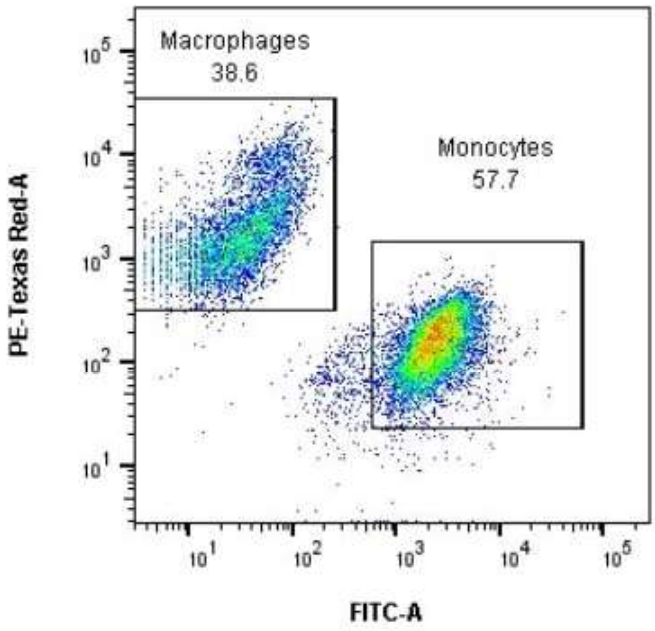

FIGURE 5.5: Scattergram of U937 monocytes and macrophages after separation.

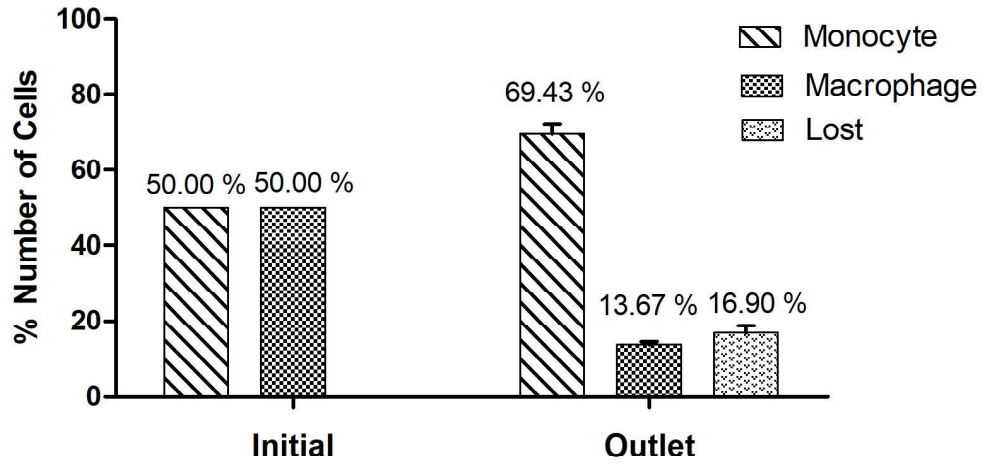

FIGURE 5.6: Separation of U937 monocytes and macrophages using 3D carbon-DEP chip.

5.4 Discussion

There was a membrane polarizability difference between the live and dead cells. Also, the conductivity and permittivity of the dead cells were not different from their surrounding DEP buffer, thus providing selective removal of the dead cells from the environment with a fluidic flow [50]. In the literature, only one other study has demonstrated the separation of live and dead monocytes [9]. A cDEP method was used for separation of live THP-1 cells from dead ones with a 95% removal efficiency. The major disadvantage of this application was cell lysis due to the high voltages required to generate DEP forces. However, using 3D carbon-DEP prevents cell damage at high voltages such as 20 Vpp. Another study separated live and dead yeast cells using reservoir-based DEP. The straightforward fabrication of reservoir-based DEP was easier compared to the 3D carbon-DEP, yet cells caused clogging in the reservoirs and the separation purity decreased [51].

Dielectrophoretic properties and separability of many cell types have been investigated using different approaches for many years. However, the investigation of cells (leukocytes) sharing the same origin (bone marrow), with similar cell surface morphologies and functional roles is highly challenging, and these studies still ongoing [52]. Other study have already examined the dielectric characteristics of leukocyte subpopulations, and some separated monocytes from B-lymphocytes, which might be expected since they possess the largest CM difference among other leukocyte subpopulations, as shown in figure 4.9 [16, 53]. Still, the separation of monocytes and macrophages, which are differentiated from these monocytes, had not been investigated and remained as a challenge before this study. One of the primary motivations for this study is that monocytes and macrophages have approximately the same cell radius and dielectric properties, meaning that the DEP-force difference occurs mainly based on the real part of the Clausius-Mossotti factor. This is why 70% separation efficiency is promising for future applications that will be conducted with patient samples maintaining highly heterogeneous cell populations which share close dielectric properties and are hard to identify with immunological labeling.

DEP method will be more popular than other cell characterization and separation methods eventually. It eliminates the many drawbacks of the existing ones.

It is a noninvasive manipulation technique, which does not require any biochemical markers and immunolabeling procedures. Thus, it does not demand any additional preparative steps and decreases the risk of changing the phenotype of the processed cells. Moreover, DEP eliminates the need for heavy and expensive equipment. Still, it needs to be improved, and devices need to be developed considering the end product so that DEP will be accepted as a universal manipulation tool.

Chapter 6

Conclusion and Future Work

In this thesis, leukocytes were characterized and separated using the 3D carbon-dielectrophoresis method. First, U937 monocytes (the human myeloid leukemia) and U937 monocyte-differentiated macrophages were characterized. The crossover frequencies of these cells were obtained as 18 kHz and 30 kHz, respectively. Dead monocytes were characterized as well, but the experimental observations showed that the dead cells were not affected by the DEP forces and stayed around the crossover regions at every frequency. Based on the obtained crossover frequencies and flow rate optimization analysis, live-dead monocytes, macrophages, and monocytes-macrophages were separated by 3D carbon-DEP. More than 90% separation efficiency was achieved for live-dead cell separations, and 70% efficiency was achieved for monocyte-macrophage separation.

Moreover, fluorescent dyes were quantitatively investigated to observe their effects on DEP responses of the cells. A slight shift in the crossover frequencies of the cells was observed when they were labeled with membrane-permeant reactive tracers. To the best of our knowledge, this was the first study that has investigated the dielectrophoretic properties of fluorescent cell tracker dyes. Finally, a new numerical tool was presented using the membrane folding factor in the Clausius-Mossotti relation to develope the DEP model realistically.

As future work, other cell populations can be characterized and separated using this 3D carbon-DEP device. For instance, the detection of rare cells has a growing importance in the advancement of medical diagnostics and personal treatment. This 3D carbon-DEP technique can be used to provide a detection system for rare cells. Identification and separation of M1 and M2 types of macrophages is also critical, and currently there are no biomarkers sufficiently identifying these cell types. M1 type macrophages, the classical type, suppress tumor cell growth, while the M2 type, an alternative type, promotes tumor cell growth. These cells almost identical phenotypically and genotypically yet have counter functions. If 3D carbon-DEP can be used to identify these subpopulations, there would be no need for biochemical labeling of these cells, and it will play a critical role in cancer diagnosis and treatment.

Bibliography

[1] H. Morgan and N. G. Green, *AC electrokinetics*. Research Studies Press,, 2003.

[2] E. O. Adekanmbi and S. K. Srivastava, "Dielectrophoretic applications for disease diagnostics using lab-on-a-chip platforms," *Lab on a Chip*, vol. 16, no. 12, pp. 2148–2167, 2016.

[3] Y. Huang, J. M. Yang, P. J. Hopkins, S. Kassegne, M. Tirado, A. H. Forster, and H. Reese, "Separation of simulants of biological warfare agents from blood by a miniaturized dielectrophoresis device," *Biomedical Microdevices*, vol. 5, no. 3, pp. 217–225, 2003.

[4] B. A. Simmons, G. J. McGraw, R. V. Davalos, G. J. Fiechtner, Y. Fintschenko, and E. B. Cummings, "The development of polymeric devices as dielectrophoretic separators and concentrators," *MRS bulletin*, vol. 31, no. 2, pp. 120–124, 2006.

[5] Y. Huang, S. Joo, M. Duhon, M. Heller, B. Wallace, and X. Xu, "Dielectrophoretic cell separation and gene expression profiling on microelectronic chip arrays," *Analytical chemistry*, vol. 74, no. 14, pp. 3362–3371, 2002.

[6] N. Mittal, A. Rosenthal, and J. Voldman, "ndep microwells for single-cell patterning in physiological media," *Lab on a Chip*, vol. 7, no. 9, pp. 1146–1153, 2007.

[7] C.-P. Jen and T.-W. Chen, "Selective trapping of live and dead mammalian cells using insulator-based dielectrophoresis within open-top microstructures," *Biomedical microdevices*, vol. 11, no. 3, p. 597, 2009.

[8] S. Bhattacharya, T.-C. Chao, N. Ariyasinghe, Y. Ruiz, D. Lake, R. Ros, and A. Ros, "Selective trapping of single mammalian breast cancer cells by insulator-based dielectrophoresis," *Analytical and bioanalytical chemistry*, vol. 406, no. 7, pp. 1855–1865, 2014.

[9] H. Shafiee, M. B. Sano, E. A. Henslee, J. L. Caldwell, and R. V. Davalos, "Selective isolation of live/dead cells using contactless dielectrophoresis (cdep)," *Lab on a Chip*, vol. 10, no. 4, pp. 438–445, 2010.

[10] S. A. Faraghat, K. F. Hoettges, M. K. Steinbach, D. R. van der Veen, W. J. Brackenbury, E. A. Henslee, F. H. Labeed, and M. P. Hughes, "High-throughput, low-loss, low-cost, and label-free cell separation using electrophysiology-activated cell enrichment," *Proceedings of the National Academy of Sciences*, p. 201700773, 2017.

[11] M. Islam, R. Natu, M. F. Larraga-Martinez, and R. Martinez-Duarte, "Enrichment of diluted cell populations from large sample volumes using 3d carbon-electrode dielectrophoresis," *Biomicrofluidics*, vol. 10, no. 3, p. 033107, 2016.

[12] A. Chow, B. D. Brown, and M. Merad, "Studying the mononuclear phagocyte system in the molecular age," *Nature Reviews Immunology*, vol. 11, no. 11, p. 788, 2011.

[13] Y. Yildizhan, U. B. Gogebakan, A. Altay, M. Islam, R. Martinez-Duarte, and M. Elitas, "Quantitative investigation for the dielectrophoretic effect of fluorescent dyes at single-cell resolution," *ACS Omega*, vol. 3, no. 7, pp. 7243–7246, 2018.

[14] Y. Yildizhan, N. Erdem, M. Islam, R. Martinez-Duarte, and M. Elitas, "Dielectrophoretic separation of live and dead monocytes using 3d carbon-electrodes," *Sensors*, vol. 17, no. 11, p. 2691, 2017.

[15] N. Erdem, Y. Yıldızhan, and M. Elitaş, "A numerical approach for dielectrophoretic characterization and separation of human hematopoietic cells," *International Journal of Engineering Research & Technology (IJERT)*, vol. 6, no. 4, pp. 1079–1082, 2017.

[16] J. Yang, Y. Huang, X. Wang, X.-B. Wang, F. F. Becker, and P. R. Gascoyne, "Dielectric properties of human leukocyte subpopulations determined by electrorotation as a cell separation criterion," *Biophysical journal*, vol. 76, no. 6, pp. 3307–3314, 1999.

[17] I.-C. Lee, J.-F. Chang, and R.-S. Juang, "Recent advances and perspectives on capture and concentration of label-free rare cells for biomedical science and engineering research," *Journal of the Taiwan Institute of Chemical Engineers*, 2018.

[18] S. Mahabadi, F. H. Labeed, and M. P. Hughes, "Dielectrophoretic analysis of treated cancer cells for rapid assessment of treatment efficacy," *Electrophoresis*, vol. 39, no. 8, pp. 1104–1110, 2018.

[19] B. D. Plouffe, M. Mahalanabis, L. H. Lewis, C. M. Klapperich, and S. K. Murthy, "Clinically relevant microfluidic magnetophoretic isolation of rare-cell populations for diagnostic and therapeutic monitoring applications," *Analytical chemistry*, vol. 84, no. 3, pp. 1336–1344, 2012.

[20] D. English and B. R. Andersen, "Single-step separation of red blood cells, granulocytes and mononuclear leukocytes on discontinuous density gradients of ficoll-hypaque," *Journal of immunological methods*, vol. 5, no. 3, pp. 249–252, 1974.

[21] W. Bonner, H. Hulett, R. Sweet, and L. A. Herzenberg, "Fluorescence activated cell sorting," *Review of Scientific Instruments*, vol. 43, no. 3, pp. 404–409, 1972.

[22] S. Miltenyi, W. Müller, W. Weichel, and A. Radbruch, "High gradient magnetic cell separation with macs," *Cytometry: The Journal of the International Society for Analytical Cytology*, vol. 11, no. 2, pp. 231–238, 1990.

[23] R. Pethig and G. H. Markx, "Applications of dielectrophoresis in biotechnology," *Trends in biotechnology*, vol. 15, no. 10, pp. 426–432, 1997.

[24] P. R. Gascoyne and J. Vykoukal, "Particle separation by dielectrophoresis," *Electrophoresis*, vol. 23, no. 13, pp. 1973–1983, 2002.

[25] B. Çetin and D. Li, "Dielectrophoresis in microfluidics technology," *Electrophoresis*, vol. 32, no. 18, pp. 2410–2427, 2011.

[26] M. Talary, K. I. Mills, T. Hoy, A. K. Burnett, and R. Pethig, "Dielectrophoretic separation and enrichment of cd34+ cell subpopulation from bone marrow and peripheral blood stem cells," *Medical and Biological Engineering and Computing*, vol. 33, no. 2, pp. 235–237, 1995.

[27] M. Stephens, M. Talary, R. Pethig, A. Burnett, and K. Mills, "The dielectrophoresis enrichment of cd34+ cells from peripheral blood stem cell harvests.," *Bone marrow transplantation*, vol. 18, no. 4, pp. 777–782, 1996.

[28] F. F. Becker, X.-B. Wang, Y. Huang, R. Pethig, J. Vykoukal, and P. Gascoyne, "Separation of human breast cancer cells from blood by differential dielectric affinity," *Proceedings of the National Academy of Sciences*, vol. 92, no. 3, pp. 860–864, 1995.

[29] A. Ismail, M. Hughes, H. Mulhall, R. Oreffo, and F. Labeed, "Characterization of human skeletal stem and bone cell populations using dielectrophoresis," *Journal of tissue engineering and regenerative medicine*, vol. 9, no. 2, pp. 162–168, 2015.

[30] H. A. Pohl, "The motion and precipitation of suspensoids in divergent electric fields," *Journal of Applied Physics*, vol. 22, no. 7, pp. 869–871, 1951.

[31] N. Abd Rahman, F. Ibrahim, and B. Yafouz, "Dielectrophoresis for biomedical sciences applications: A review," *Sensors*, vol. 17, no. 3, p. 449, 2017.

[32] V. Raicu, G. Raicu, and G. Turcu, "Dielectric properties of yeast cells as simulated by the two-shell model," *Biochimica et Biophysica Acta (BBA)-Bioenergetics*, vol. 1274, no. 3, pp. 143–148, 1996.

[33] R. Pethig, "Dielectrophoresis: Status of the theory, technology, and applications," *Biomicrofluidics*, vol. 4, no. 2, p. 022811, 2010.

[34] S. K. Srivastava, A. Gencoglu, and A. R. Minerick, "Dc insulator dielectrophoretic applications in microdevice technology: a review," *Analytical and bioanalytical chemistry*, vol. 399, no. 1, pp. 301–321, 2011.

[35] H. Shafiee, J. L. Caldwell, M. B. Sano, and R. V. Davalos, "Contactless dielectrophoresis: a new technique for cell manipulation," *Biomedical microdevices*, vol. 11, no. 5, p. 997, 2009.

[36] M. Hashimoto, H. Kaji, and M. Nishizawa, "Selective capture of a specific cell type from mixed leucocytes in an electrode-integrated microfluidic device," *Biosensors and Bioelectronics*, vol. 24, no. 9, pp. 2892–2897, 2009.

[37] P. R. Gascoyne, X.-B. Wang, Y. Huang, and F. F. Becker, "Dielectrophoretic separation of cancer cells from blood," *IEEE transactions on industry applications*, vol. 33, no. 3, pp. 670–678, 1997.

[38] A. Aghilinejad, M. Aghaamoo, and X. Chen, "Numerical study of joule heating effect on dielectrophoresis-based circulating tumor cell separation," in *ASME 2017 International Mechanical Engineering Congress and Exposition*, pp. V003T04A014–V003T04A014, American Society of Mechanical Engineers, 2017.

[39] R. Martinez-Duarte, P. Renaud, and M. J. Madou, "A novel approach to dielectrophoresis using carbon electrodes," *Electrophoresis*, vol. 32, no. 17, pp. 2385–2392, 2011.

[40] M. d. C. Jaramillo, E. Torrents, R. Martínez-Duarte, M. J. Madou, and A. Juárez, "On-line separation of bacterial cells by carbon-electrode dielectrophoresis," *Electrophoresis*, vol. 31, no. 17, pp. 2921–2928, 2010.

[41] R. Martinez-Duarte, F. Camacho-Alanis, P. Renaud, and A. Ros, "Dielectrophoresis of lambda-dna using 3d carbon electrodes," *Electrophoresis*, vol. 34, no. 7, pp. 1113–1122, 2013.

[42] G. Mernier, R. Martinez-Duarte, R. Lehal, F. Radtke, and P. Renaud, "Very high throughput electrical cell lysis and extraction of intracellular compounds using 3d carbon electrodes in lab-on-a-chip devices," *Micromachines*, vol. 3, no. 3, pp. 574–581, 2012.

[43] B. M. Sharp, "Conversion of the u937 monocyte into" macrophage-like" populations exhibiting m1 or m2 characteristics," 2013.

[44] T. Monie, *The Innate Immune System: A Compositional and Functional Perspective*. Academic Press, 2017.

[45] M. Jönsson, K. Welch, S. Hamp, and M. Strømme, "Bacteria counting with impedance spectroscopy in a micro probe station," *The Journal of Physical Chemistry B*, vol. 110, no. 20, pp. 10165–10169, 2006.

[46] H. P. Schwan, "Electrical properties of tissue and cell suspensions," in *Advances in biological and medical physics*, vol. 5, pp. 147–209, Elsevier, 1957.

[47] B. H. Lapizco-Encinas, B. A. Simmons, E. B. Cummings, and Y. Fintschenko, "Dielectrophoretic concentration and separation of live and dead bacteria in an array of insulators," *Analytical chemistry*, vol. 76, no. 6, pp. 1571–1579, 2004.

[48] K. R. Foster, F. A. Sauer, and H. P. Schwan, "Electrorotation and levitation of cells and colloidal particles," *Biophysical journal*, vol. 63, no. 1, pp. 180–190, 1992.

[49] P. R. Gascoyne and S. Shim, "Isolation of circulating tumor cells by dielectrophoresis," *Cancers*, vol. 6, no. 1, pp. 545–579, 2014.

[50] E. Prodan, C. Prodan, and J. H. Miller Jr, "The dielectric response of spherical live cells in suspension: an analytic solution," *Biophysical journal*, vol. 95, no. 9, pp. 4174–4182, 2008.

[51] S. Patel, D. Showers, P. Vedantam, T.-R. Tzeng, S. Qian, and X. Xuan, "Microfluidic separation of live and dead yeast cells using reservoir-based dielectrophoresis," *Biomicrofluidics*, vol. 6, no. 3, p. 034102, 2012.

[52] D. R. Gossett, W. M. Weaver, A. J. Mach, S. C. Hur, H. T. K. Tse, W. Lee, H. Amini, and D. Di Carlo, "Label-free cell separation and sorting in microfluidic systems," *Analytical and bioanalytical chemistry*, vol. 397, no. 8, pp. 3249–3267, 2010.

[53] X.-B. Wang, J. Yang, Y. Huang, J. Vykoukal, F. F. Becker, and P. R. Gascoyne, "Cell separation by dielectrophoretic field-flow-fractionation," *Analytical chemistry*, vol. 72, no. 4, pp. 832–839, 2000.